The neurotrophic factor MANF regulates autophagic flux and lysosome function to promote proteostasis in *C. elegans*

Shane Taylor and Bhagwati P Gupta*
Department of Biology, McMaster University, Hamilton, ON L8S-4K1, Canada

*Author for Correspondence.
Email: guptab@mcmaster.ca; Phone: 1-905-525-9140 x26451

Running title: MANF-1 role in lysosomes and proteostasis

Keywords: MANF, MANF-1, *C. elegans*, autophagy, lysosome, ER stress, ER-UPR, Unfolded protein response, proteostasis, dopaminergic neuron, aging

ABTRACT

The neurotrophic factor, Mesencephalic Astrocyte Derived Neurotrophic Factor (MANF), promotes neuronal health and survival. MANF is conserved in metazoans and necessary for the protection of dopaminergic neurons. The neuroprotective role of MANF involves regulation of the ER unfolded protein response (ER-UPR). Recent work has shown that MANF also functions in many other tissues and affects autophagy genes. Previously, we reported that *C. elegans manf-1* mutants show defects including increased ER stress, α-Synuclein aggregation, and age-dependent dopaminergic neurodegeneration. In this study, we have further investigated manf-1's function and describe its mechanism of action in regulating stress response, protein aggregation and aging. Our results showed that exposure to ER stress-inducing agents caused *manf-1* transcription and protein expression to be upregulated. Consistent with the protective role of *manf-1*, mutant animals showed greater sensitivity to ER stress and died prematurely. We generated *manf-1p::manf-1::mCherry* (*MANF-1*^{OE}) and *hsp::manf-1* transgenic strains overexpressing MANF and found that these animals had an extended lifespan, reduced protein aggregation, and increased neuronal health. The *in vivo* analysis of MANF-1 expression revealed that the protein was secreted and present in many tissues. Subcellular studies showed that MANF-1 was localized to lysosomes. We also observed that MANF-1^{OE} worms had reduced LGG-1 and SQST-1/p62 levels, and increased expression and nuclear localization of the autophagy transcription factor *hlh-30/*TFEB. Thus, MANF-1 regulates protein homeostasis through increased lysosome activity and autophagic flux. Collectively, our work provides a novel understanding of MANF-1 function in promoting neuronal health, stress response, proteostasis, and lifespan of animals.

INTRODUCTION

Nothing is perfect, and this includes the intracellular machinery of a cell. Despite constantly working, the ability of the cell to maintain homeostasis declines with age (Taylor and Dillin 2011). Dysregulated homeostasis can cause proteins to misfold and become clumps or aggregates. Abnormal accumulation of protein aggregates is toxic to cells as it increases cellular stress, disrupts physiological processes, and eventually results in a failure of cells, tissues, and organs to maintain their function. Current research suggests that maintaining protein homeostasis (proteostasis) is essential for the functioning of cellular processes, reducing age-related diseases, and promoting healthy aging. Fortunately, cells are capable of activating stress response signaling pathways such as the unfolded protein response (UPR) to maintain proteostasis and minimize cellular damages. In most cases, these responses work very well but they are not always efficient. One consequence of a failure to eliminate toxic protein aggregates is the development of age-related diseases, including neurodegenerative diseases such as Parkinson's

Disease (PD) and Huntington's Disease (HD) (Taylor and Dillin 2011; Remondelli and Renna 2017; Hetz and Saxena 2017; Remondelli and Renna 2017).

A promising approach to enhancing proteostasis to protect against neurodegeneration involves the use of Neurotrophic factors (NTFs). NTFs are a class of proteins that support the survival, growth, and differentiation of neuronal cells. Their anti-inflammatory and anti-apoptotic properties make them promising therapeutic candidates for the treatment of neurodegenerative diseases (Nasrolahi et al. 2018). One family of NTFs that is relevant to this study, is represented by two proteins, namely cerebral dopamine neurotrophic factor (CDNF) and the mesencephalic astrocyte-derived neurotrophic factor (MANF) (Pakarinen and Lindholm 2023). CDNF and MANF are paralogues that are structurally and mechanistically distinct from other classical NTFs (Lindahl et al. 2017; Nasrolahi et al. 2018). Whereas vertebrates contain both CDNF and MANF, only MANF is present in invertebrates. Both these factors have neurotrophic activity and protect dopaminergic (DA) neurons in different animal models (Pakarinen and Lindholm 2023). MANF levels decline with age, a phenomenon that negatively correlates with progressive increase in PD and PD-like symptoms in older adults (Voutilainen et al. 2015; Richman et al. 2018; Sousa-Victor et al. 2019).

MANF homologs have been examined in different animals including mouse, rat, and two leading invertebrate models, *Drosophila melanogaster* and *C. elegans*. These studies have shown that the cytoprotective ability of MANF involves ER-UPR regulation (Pakarinen and Lindholm 2023). The ER-UPR is a quality control mechanism that works to rectify cellular stress by correctly folding misfolded proteins, reducing translation, and activating apoptosis when homeostasis cannot be restored (Walter and Ron 2011). The ER-UPR has three conserved transmembrane proteins, inositol-requiring enzyme 1 (IRE1), protein kinase RNA (PKR)-like ER kinase (PERK), and activating transcription factor 6 (ATF6) (*ire-1*, *pek-1*, and *atf-6*, respectively, in *C. elegans*), that activate overlapping but distinct pathways in response to stress (Walter and Ron 2011; Hetz et al. 2013). Additionally, IRE1 creates a spliced form of the transcription factor X-Box binding protein-1 (XBP1), the main regulator of the ER-UPR. Spliced XBP-1 works to maintain homeostasis through transcription of chaperones such as GRP78/BiP (*C. elegans hsp-4*), which is affected by MANF (Walter and Ron 2011; Hetz et al. 2013; Taylor and Hetz 2020; Eesmaa et al. 2021; Kovaleva et al. 2023). Consistent with its role in ER-UPR maintenance, MANF sequence contains an ER retention signal and is shown to localize to the ER (Lõhelaid et al. 2022). Under normal conditions, MANF is thought to be retained in the ER and is secreted in response to protein misfolding or cellular stress (Jäntti and Harvey 2020).

Recent work has shown that MANF is also involved in other diseases with dysregulated homeostasis, more specifically metabolic dysfunction, diabetes, ischemia, and retinal degeneration (Neves et al. 2016; Nasrolahi et al. 2018; Sousa-Victor et al. 2019). Consistent with these data, MANF is expressed in many tissues and is needed to maintain cellular homeostasis

(Neves et al. 2016; Danilova, Belevich, et al. 2019; Sousa-Victor et al. 2019; Peled et al. 2021). How MANF affects so many different processes is not understand. Is there a common mechanism of its action to confer protection in distinct tissues or the protein functions differently in different tissues?

In this regard, the nematode *C. elegans* offers the necessary genetic and molecular tools to investigate the function of MANF (Brenner 1974; Corsi et al. 2015; Liang et al. 2020). Studies on the *C. elegans* MANF homolog, MANF-1, have shown that it is a secreted protein that is endocytosed upon binding to sulfatides leading to a cytoprotective response (Bai et al. 2018). Work from our group and others has provided further understanding of the function of MANF-1 that includes age-dependent protection of DA neurons (Richman et al. 2018), regulation of the ER-UPR chaperone HSP-4/BIP/GRP78, inhibition of α-Synuclein aggregation, and sensitivity to bacterial pathogenesis (Richman et al. 2018; Zhang et al. 2018; Hartman et al. 2019). The protective role of *manf-1* may be mediated by genes involved in autophagy, ER-UPR, and immunity (Zhang et al. 2018; Hartman et al. 2019).

This study focuses on the mechanism of MANF-1 function in *C. elegans*. Our characterization of *manf-1* mutants revealed essential roles of the gene in regulating ER stress and ER-UPR pathways. We generated multiple transgenic strains overexpressing MANF-1 (*hsp::manf-1* and *manf-1p::manf-1::mCherry*) and found these animals to have a longer lifespan, improved proteostasis, and reduced neurodegeneration. Consistent with these findings, MANF-1::mCherry chimeric protein was ubiquitously expressed and secreted. Colocalization studies using a set of subcellular markers revealed MANF-1's novel localization to lysosomes. Further characterization of *manf-1p::manf-1::mCherry* (MANF-1^{OE}) animals using LGG-1 and p62/SQST-1 reporters showed a reduction in autophagosome formation and increased autophagic flux. Moreover, HLH-30/TFEB transcription factor that regulates autophagy and lysosome biogenesis was upregulated and nuclear localized, suggesting that the cytoprotective ability of *MANF-1* was dependent on HLH-30/TFEB. Among other changes, lipid metabolism was reduced in MANF-1^{OE} animals, which agrees with increased autophagy and the lysosomal activity. Altogether, our findings establish MANF-1 as being more than a neurotrophic factor, but rather a player regulating the ER-UPR, autophagy, and lysosomal function, potentially in a well co-ordinated manner, to maintain proteostasis, neuronal health and lifespan of animals.

Results

ER stress activates *manf-1* expression and affects viability and lifespan of *manf-1* mutants

We had earlier characterized the role of *C. elegans manf-1* using mutant strains and a transgenic line carrying *manf-1p::GFP* (Richman et al. 2018). As the next step, *manf-1p::GFP* expression

was examined following treatment with the ER stress-activating drug, tunicamycin. The results showed a significant increase in GFP fluorescence (**Fig. 1A**). Consistent with this, *manf-1* transcription was upregulated in animals subjected to acute and chronic tunicamycin treatments (**Fig. 1B and C**). We also used an endogenously tagged *manf-1::mKate2* strain (Hartman et al. 2019) and observed that tunicamycin caused more than 100-fold increase in fluorescence (**Fig. 1D**). Thus, *manf-1* acts as an ER stress sensor and is upregulated to confer protection in animals.

Earlier, we and others had shown that *manf-1* mutants have increased expression of *hsp-4* (Bai et al. 2018; Richman et al. 2018; Hartman et al. 2019). Since ER-UPR is known to decline with age (Taylor and Dillin 2011; Taylor and Dillin 2013), the effect of MANF-1 was examined in older worms. To this end, *manf-1(tm3603)* animals were treated with tunicamycin and *hsp-4p::GFP* levels were quantified in day one, four, and seven old adults. The results showed that additional ER stress induction using tunicamycin caused a further upregulation of both GFP fluorescence and *hsp-4* transcripts with age (**Fig. 1E-H**). Together with previous reports of higher *hsp-4p::GFP* reporter in *manf-1* mutant larvae and day 1 adults (Richman et al. 2018; Hartman et al. 2019), these data led us to conclude that *manf-1* is essential for the ER-UPR maintenance throughout the life time of animals. The crucial role of the neurotrophic factor was demonstrated by additional experiments, showing that mutations in *manf-1* significantly reduced the lifespan of animals **(Fig. 1I)**. Furthermore, we found that a chronic exposure of tunicamycin enhanced neurodegeneration (**Fig. S1A**) and caused a significant reduction in the lifespan **(Fig. 1J).** In line with this, an acute treatment significantly increased the lethality of *manf-1(tm3603)* animals (**Fig. 1K**).

Finally, we examined whether *manf-1* affects the sensitivity of animals towards other forms of stress. To this end, heat and oxidative stress treatment assays were carried out. There was no change in the response of *manf-1* mutants compared to wildtype (**Fig. S1B and C**) except for the chronic effect of paraquat on neurons at day 3 of adulthood (**Fig. S1D)**. Taken together, results presented in this section demonstrate that *manf-1* is necessary for the maintenance of ER-UPR and plays an essential role in protecting animals against ER stress.

manf-1 **interacts with ER-UPR components and mutants show enhanced protein aggregation defects**

The regulation of *hsp-4* in *manf-1(tm3603)* animals led us to investigate the ER-UPR genes that define each of the signaling arms, namely ATF6/*atf-6*, PERK/*pek-1*, IRE1/*ire-1*, and the downstream transcription factor XBP-1/*xbp-1* (Walter and Ron 2011; Hetz et al. 2013; Hartman et al. 2019; Taylor and Hetz 2020). The expression of all four genes was significantly upregulated in *manf-1* mutants **(Fig. 2A)**. The ratio of spliced to total *xbp-1* was also high (**Fig. 2B**). These data suggest that *manf-1* affects a wide range of processes to maintain ER homeostasis.

Since ER stress affects protein folding and degradation, we examined proteostasis defects in *manf-1* mutants. To this end, transgenic animals expressing human α-Synuclein in body wall muscles were used, which we had examined earlier and demonstrated increased aggregation in the absence of *manf-1* (Richman et al. 2018). Analysis of α-Synuclein::GFP in day 1, 4 and 7 old *manf-1(tm3603)* adults revealed a higher aggregation compared to controls (**Fig. 2C**), suggesting that *manf-1* is necessary to maintain proteostasis. The phenotype was further enhanced by RNAi knockdowns of *atf-6* and *pek-1* (**Fig. 2D-G**), providing evidence for ER-UPR being compromised but not eliminated in the absence of *manf-1*. Surprisingly, *manf-1(tm3603); xbp-1*(RNAi) animals showed an opposite effect, i.e., α-Synuclein levels were greatly reduced (**Fig. 2D-G**). While the precise reasons are unknown, we noted that animals were unhealthy and exhibited slower growth, abnormal movement, reduced viability, and a tendency to frequently burst open through vulval opening (see Methods) (**Fig. S2A & B**). Therefore, it is conceivable that *xbp-1* knockdown had a severely detrimental effect on *manf-1* mutants leading to a reduction in α-Synuclein abundance. The synthetic interaction between *manf-1* and *xbp-1* is consistent with a previous report showing *manf-1* and *ire-1* double mutants and *manf-1* mutants treated with *xbp-1* RNAi being lethal or sterile (Hartman et al. 2019).

We used another protein aggregation system to examine the effect of *manf-1*, which consisted of polyQ repeats that serves as a *C. elegans* Huntington's Disease model (Morley et al. 2002). To this end, two different polyQ strains, Q35::YFP (AM140) and Q40::YFP (AM141), were used (Morley et al. 2002). Similar to the α-Synuclein, both polyQ expressing worms showed a significant increase in protein aggregation in *manf-1* mutant background compared to wildtype **(Fig. 2H, I and K, Fig. S3)**. The thrashing defects of polyQ35 animals were also enhanced **(Fig. 2J)**. Combined with the above α-Synuclein results, these data demonstrate that *manf-1* is necessary for the ER-UPR regulation and maintenance of proteostasis.

Overexpression of *manf-1* reduces protein aggregation, improves neuronal survival, and extends lifespan

The above data showing that *manf-1* is essential for the stress response maintenance and proteostasis led us to reason that overexpression of the gene is likely to be protective. To test this hypothesis, we took different approaches to activate *in vivo* expression of *manf-1*. One of these included treating animals to bioactive compounds curcumin and lithium that, similar to studies in mammalian systems (Abu-Hijleh et al. 2020), increased *manf-1* levels but only modestly (Taylor and Gupta, in prep). Other approaches involved generating two different transgenic strains, one of which (*hsp::manf-1*) contained *manf-1* cDNA under the control of a heat shock promoter and the other (m*anf-1p::manf-1::mCherry*) carried *manf-1* genomic DNA along with the endogenous promoter (see Methods).

For the *hsp::manf-1* strain, we tested whether inducing *manf-1* expression will have cytoprotective effects on animals. The strain was responsive to heat treatments since a 1 hr 31°C

exposure caused a significant increase in *manf-1* transcription in day 1 adults (**Fig. 3A**). Interestingly, no heat shock was needed at later stages to activate *manf-1* since day 3 and day 7 adults showed significantly higher levels of expression without any treatments (**Fig. 3B**). This may be due to transcripts accumulating in older adults due to leaky expression at the room temperature. Additionally, the basal activation may cause transcript levels to become effectively higher over time in transgenic animals compared to N2 controls since *manf-1* expression is known to decline with age (Richman et al. 2018).

Phenotypic analysis of day 7 *hsp::manf-1* adults showed increased protection of DA neurons with or without heat treatments. Specifically, the animals had a higher proportion of neurons with normal looking dendritic processes and cell bodies (**Fig. 3C**). Quantification of neuronal defects revealed fewer animals with both defective dendritic and cell body morphologies, demonstrating *manf-1*'s beneficial effects on promoting neuronal health. The day 7 transgenic adults showed a significant reduction in α-Synuclein::YFP fluorescence, suggesting a decrease of protein aggregation defects in older animals (**Fig. 3D**). The lifespan of *hsp-manf-1* animals was also significantly enhanced (roughly 5% in heat-treated and 21% in untreated animals; see Supplementary Table 1; **Fig. 3E**).

We next examined the phenotype of *manf-1p::MANF-1::mCherry* (referred to as *MANF-1*^{OE}*)* transgenic animals. Three different lines were generated that had *manf-1* transcript levels ranging from 3x to 6x (**Fig. S4A**, also see Methods). One of these (DY759) was selected for more detailed analysis. The examination of *hsp-4* expression showed that while transcript level was not significantly affected (**Fig. S4A)**, *MANF-1*^{OE} animals exhibited a modest increase in GFP fluorescence, suggesting that ER-UPR was weakly activated (**Fig. 4A & B)**. More importantly, *MANF-1*^{OE} suppressed the ER stress phenotype of *manf-1(tm3603)* animals based on the *hsp-4p::GFP* analysis (**Fig. 4A & B)**. Interestingly, the animals showed an increase in both, total and spliced, *xbp-1* transcript levels (**Fig. S4A)**.

To determine if *MANF-1*^{OE} had protective capabilities, we analyzed the DA neuron morphology, α-Synuclein and polyQ35 aggregation, movement, and lifespan of animals. The results showed that *manf-1* overexpression conferred a significant protection on DA neurons (**Fig. 4D**) and reduced aggregation of α-Synuclein (**Fig. 4E**) and polyQ35 (**Fig. 4G, H, J)**. Additionally, *MANF-1*^{OE} caused improved thrashing response of the polyQ35 expressing worms **(Fig. 4I**). We also found that *MANF-1*^{OE} animals had a significant increase in lifespan (19.2% higher mean lifespan; 19.9 ± 0.5 days SEM compared to 16.7 ± 0.4 days for controls, **Supplementary Table 1**) although their resistance to acute ER stress was comparable to wildtype **(Fig. 4K, L**). Overall, these results demonstrate the multiple beneficial effects of *MANF-1*^{OE} in *C. elegans*.

MANF-1 is secreted and localized to lysosomes

The *MANF-1*^{OE} transgenic strain was used to study the *in vivo* localization of the chimeric protein. Earlier, we and others had reported that *manf-1* is expressed ubiquitously from the egg stage till adulthood in tissues such as the pharynx, hypodermis, and intestine (Richman et al. 2018; Hartman et al. 2019). The MANF-1::mCherry in *MANF-1*^{OE} animals was localized to many of the same regions as well as in areas such as coelomocytes and the extracellular space (**Fig. 5A-D**). These data confirm that MANF-1 is a secreted protein.

Further examination of MANF-1 expression revealed puncta-like structures in hypodermal cells, which were confirmed to be lysosomes based on colocalization studies using markers for various subcellular regions. Specifically, the MANF-1::mCherry pattern matched perfectly with the lysosomal dye Lysotracker Green and the lysosomal membrane marker *scav-3::GFP* (Li et al. 2016) (**Fig. 5E**). Within coelomocytes, MANF-1's localization to lysosomes was confirmed using the marker *lmp-1::GFP* (Treusch et al. 2004) (**Fig. 5E**). As reported earlier for lysosomes (Sun et al. 2020), MANF-1 positive structures showed changes with age from a vesicular to tubular-like morphology (**Fig. 5F & G**). *manf-1::mCherry* did not show overlap with *rme-8::GFP* (endosomes) (Zhang et al. 2001), *MANS::GFP* (golgi body) (Treusch et al. 2004), and *lgg-1p::GFP::lgg-1* (autophagosomes) (Lapierre et al. 2011) (**Fig. 5E**, **Fig S5A**). Additionally, we did not observe MANF-1::mCherry in other regions such as mitochondria (*myo-3p::GFP(mit)*) (Labrousse et al. 1999) (**Fig S5B**), ER (*vha-6p::GFP::C34B2.10*)(Xu et al. 2012) (**Fig S5C**), and lipid droplets (Bodipy 493/503) (**Fig S5D**). Finally, *manf-1::mCherry* was not detected in neurons based on the DA neuron marker *dat-1p::YFP* and pan-neuronal marker *unc-119p::GFP* (Altun-Gultekin et al. 2001) (**Fig S5E, F**).

To further support MANF-1 localization to lysosomes, we examined three additional, independently generated transgenic strains. Two of these, DY798 and DY800, carried lower concentrations of the *manf-1p::manf-1::mCherry* plasmid compared to DY759 (DY798: 3x lower; DY800: 30x lower; see Methods). The third strain, NK2548 (*manf-1::mKate2*), contains the *mKate2* reporter, inserted in-frame at the 3' end of the endogenous *manf-1* using CRISPR (Hartman et al. 2019). While the DY798 and DY800 animals showed weak fluorescence, the pattern was identical to that described above (data not shown). In the case of NK2548, MANF-1::mKate2 fluorescence was barely detectable but observed in lysosomes when animals were treated with tunicamycin and stained with Lysotracker Green (**Fig. 5H**).

Altogether, the results described above demonstrate that MANF-1 is a secreted protein and localizes to lysosomes, suggests the possibility that it may interact with other lysosomal membrane proteins to regulate lysosome-mediated proteostasis.

MANF-1 promotes autophagy and lysosome function

The analysis of *manf-1* expression pattern along with mutant and overexpression studies, suggests the essential role of this gene in maintaining the stress response and proteostasis

through mechanisms that may involve lysosomes. Thus, MANF-1 may regulate lysosome function to promote autophagy, helping to clear misfolded and aggregated proteins. To investigate this further, we examined factors involved in the autophagic process. The results showed that *MANF-1*^{OE} enhanced nuclear localization of HLH-30/TFEB, a transcription factor known as a regulator of autophagy and lysosomal genes in *C. elegans* (Lapierre et al. 2013) (**Fig. 6A&E**). Additionally, the expression of *hlh-30* was upregulated in *MANF-1*^{OE} animals (**Fig. 6B**). Two additional autophagy genes, *lgg-1/LC3* and *sqst-1/*p62, were examined. LGG-1 is involved in autophagosome formation and SQST-1 is an autophagy receptor that facilitates degradation of ubiquitinated protein cargo (Kumsta et al. 2019; Ploumi et al. 2021). The results showed that while transcript levels of *lgg-1/LC3* and *sqst-1/*p62 were unaffected in *MANF-1*^{OE} worms (**Fig. 6B**), there was a significant reduction in LGG-1::GFP and SQST-1::GFP fluorescent puncta in seam cells and pharynx, respectively (**Fig. 6C&F, D&G**), consistent with increased autophagic clearance (Yeawon Kim et al. 2023). We concluded that beneficial effects of MANF-1 overexpression are mediated through enhanced autophagy and lysosomal function.

The essential role of *hlh-30* in *manf-1* function was further supported by the analysis of *hlh-30(tm1978); MANF-1*^{OE} double mutant. We found that in the absence of *hlh-30*, *MANF-1*^{OE} animals had a reduction in the size of MANF-1::mCherry puncta (**Fig. 6H & I**), a slower thrashing rate (**Fig. 6J**) and a shorter lifespan (**Fig. 6K**), suggesting that *MANF-1*^{OE} mediates its effect through HLH-30. As MANF-1 functions in an HLH-30-dependent manner and HLH-30 affects lipid droplet clearance (Settembre et al. 2013), we investigated whether lipid content was affected by *manf-1*. Using Oil Red O to analyze lipids, *manf-1(tm3603)* animals showed high lipid levels (**Fig. 6L**). An opposite phenotype was observed in *MANF-1*^{OE} animals, causing a reduction in lipid level, lipid droplet size, and quantity of lipid droplets (**Fig. 6M-P**). Overall, these data demonstrate that *manf-1* utilizes *hlh-30* to regulate autophagy and lysosome function in *C. elegans*.

DISCUSSION

The neurotropic factor MANF was originally identified for its role in promoting dopaminergic neuron survival but subsequently found to be also involved in many other processes (Petrova et al. 2003; Voutilainen et al. 2009; Neves et al. 2016; Nasrolahi et al. 2018; Sousa-Victor et al. 2019). Studies on MANF's mechanism of action revealed the protein is localized to the ER and necessary for ER-UPR maintenance. Expression studies of MANF in animal models have reported ubiquitous expression in many tissues and its presence in both intracellular and extracellular environments (Lindholm et al. 2008; Palgi et al. 2012; Henderson et al. 2013; Bai et al. 2018; Danilova, Galli, et al. 2019).While intracellular MANF appears to affect ER-UPR function, the secreted MANF may utilize mechanisms that are neither fully understood nor limited to ER maintenance (Lõhelaid et al. 2022).

We and others reported earlier that the *C. elegans* MANF homolog, MANF-1, plays essential roles in protecting dopaminergic neurons and ER stress maintenance (Bai et al. 2018; Richman et al. 2018; Hartman et al. 2019). In this study, we present a novel understanding of MANF function in the maintenance of stress response, proteostasis, and longevity. We found that *manf-1* expression was increased in response to ER stress, which agrees well with studies in other systems such as *drosophila*, mice and cell lines (Tadimalla et al. 2008; Glembotski et al. 2012; Lindström et al. 2016; Xu et al. 2019; Eesmaa et al. 2021). Additionally, *manf-1* mutants showed chronic ER-UPR activation and when subjected to ER stress, they exhibited enhanced neurodegeneration and a shorter lifespan. Since the ER-UPR activation helps cells to manage stress through multiple mechanisms including enhanced protein folding and clearance of non-functional proteins (Walter and Ron 2011; Hetz et al. 2013), we examined whether *manf-1* mutant animals have defects in these processes. The results showed increased protein aggregation in PD and HD models that express human α-Synuclein and polyQ, respectively. The phenotypes were exacerbated in older adults and contributed to locomotion defects, suggesting age-dependent loss of proteostasis maintenance in animals lacking *manf-1*.

Our work demonstrates that overexpression of *manf-1* through different paradigms offers cytoprotective benefits and promotes healthy aging. We used multiple approaches to activate *manf-1* expression and demonstrated that high levels of MANF-1 reduced protein aggregation, improved mobility, protected dopaminergic neurons, and extended the lifespan of animals. Consistent with such broad beneficial effects, we found that MANF-1 was broadly expressed at different stages and in different cell types. The transgenic animals showed high levels of expression in the head around the pharynx, an area that contains many neurons including dopaminergic neurons. While we did not see an obvious overlap between MANF-1-expressing cells and neurons, the presence of MANF-1 in other nearby cells may confer neuroprotection given the protein's extracellular role which allows it to be efficiently taken up by cells (Bai et al. 2018).

The subcellular analysis of MANF-1 expression revealed that the protein is predominantly localized to lysosomes of the pharynx, hypodermal cells and coelomocytes. In addition, MANF-1 was found to be present in the extracellular environment. This novel expression pattern suggests potential mechanisms for how MANF-1 may elicit its cytoprotective function. Proteins in coelomocytes, which are scavenger cells, play roles in efficient uptake of materials from the pseudocoelom and endosomal to lysosomal trafficking (Fares and Greenwald 2001). Following the uptake by coelomocytes, molecules travel through the endocytic compartments eventually going to lysosomes for degradation (Gee et al. 2017). While the exact mechanism of MANF-1 role in coelomocytes is unknown, it is likely to affect lysosome function to maintain proteostasis. In support of this, Sousa et al. recently reported GO enrichment for lysosomal and endosomal terms in MANF deficient macrophages (Sousa et al. 2023 Mar 23). The authors also showed that

recombinant MANF in older adults improved phagocytosis-induced lysosomal activity (Sousa et al. 2023 Mar 23).

Recent studies have revealed that lysosomes act as signaling hubs inside the cell and dysregulation of lysosomal function and autophagy are associated with various defects and neurodegenerative diseases (Bonam et al. 2019; Lawrence and Zoncu 2019). The autophagic-lysosomal pathway is instrumental in clearing the toxic protein aggregates. A complex protein network involving mTOR and AMPK and more specifically the transcription factor HLH-30/TFEB, which is a regulator of lysosomal and autophagy genes, has been a focal point of research in the lysosomal pathway (Napolitano and Ballabio 2016; Carroll and Dunlop 2017; Carosi et al. 2022). We found that MANF-1^{OE} affects the gene expression and nuclear localization of HLH-30/TFEB. HLH-30 is necessary for the lifespan extension conferred by Insulin/IGF-1 Signaling and other longevity pathways (Lapierre et al. 2013). We found that HLH-30 is also essential for the movement and lifespan of MANF-1^{OE} animals. Studies have shown that calcium released from lysosomes can activate calcineurin to dephosphorylate TFEB leading to its nuclear localization (Napolitano and Ballabio 2016). Additionally, lysosomal calcium can trigger ER calcium release and signaling (Napolitano and Ballabio 2016; Bonam et al. 2019). These data, together with observations that changes in ER calcium can promote MANF secretion, lead us to suggest that MANF is part of a network to facilitate ER and lysosome crosstalk to regulate TFEB-mediated activation of autophagy and proteostasis. Interestingly, we observed a reduction in the size of MANF-1-positive foci in *hlh-30* mutants, raising the possibility of a feedback mechanism. In agreement with this, *manf-1* promoter contains sequences overlapping with HLH-30 CLEAR binding motif. Thus, it is conceivable that similar to lysosomal gene targets of TFEB (Lapierre et al. 2013), *manf-1* is transcriptionally regulated by *hlh-30* and forms a positive regulatory network.

The role of MANF-1 in lysosome-mediated signaling and involvement of HLH-30/TFEB in this process led us to investigate the roles of LGG-1/Atg8/LC3 and SQST-1/p62 that regulate autophagy (Palmisano and Meléndez 2016; Henis-Korenblit and Meléndez 2019; Ploumi et al. 2021; Ploumi et al. 2023). While an increase in LGG-1 and SQST-1 puncta may be caused by a block in autophagy (Palmisano and Meléndez 2016; Henis-Korenblit and Meléndez 2019; Ploumi et al. 2021; Ploumi et al. 2023), a reduction in both is indicative of an increase in autophagic flux. We found that MANF-1^{OE} animals had reduced LGG-1::GFP and SQST-1::GFP puncta, suggesting that MANF-1 promotes autophagy. Consistent with these data, a recent study reported that MANF overexpression in mouse kidney cells promoted autophagy and mitochondrial biogenesis (Yeawon Kim et al. 2023). The authors also observed a decrease in p62 abundance and identified p-AMPK and FOXO3 playing roles in promoting mitochondrial biogenesis. Whether *C. elegans* AAK-2/AMPK and DAF-16/FOXO are also involved in MANF-1-mediated processes remains to be investigated.

Since ER-UPR, autophagy, and lysosomes affect lipid metabolism (Singh et al. 2009; Moncan et al. 2021; Xu and Taubert 2021), we assessed whether MANF-1 is also involved in this process. The examination of neutral lipids revealed increased levels in *manf-1* mutants. As expected, the MANF-1^{OE} animals had an opposite phenotype, which was accompanied by a reduction in the number and size of lipid droplets. Earlier, TFEB was shown to be involved in the clearance of lipid droplets, regulating lipid catabolism (Napolitano and Ballabio 2016). Related to this, TFEB and HLH-30 were shown to regulate lysosomal genes and fusion of lipid droplets to lysosomes in a process called lipophagy (O'Rourke and Ruvkun 2013; Settembre et al. 2013). Whether the lipid phenotype of *MANF-1^{OE}* involves activation of HLH-30/TFEB-mediated signaling is unknown.

In conclusion, the findings presented in this paper provide a new understanding of the role of MANF in proteostasis maintenance. Future work is needed to identify cellular components that interact with MANF to regulate lysosome function, autophagy, and stress response leading to beneficial effects in neurons, aggregation and longevity.

ACKNOWLEDGEMENTS

This work was supported by the Natural Sciences and Engineering Research Council of Canada Discovery grant to B.P.G. Some of the strains were obtained from the *Caenorhabditis* Genetics Center, which is funded by the NIH Office of Research Infrastructure Programs (P40 OD010440). The pGLC130 plasmid was made by Komal Prajapati. We thank WormBase for its citation database on individual genes (PMID 19910365) and the McMaster biology department confocal resource for assistance with imaging. Ram Mishra and Ravi Selvaganapathy provided feedback on some of the experiments.

AUTHOR CONTRIBUTIONS

S.K.B.T. carried out the experiments and generated many reagents for the study. S.K.B.T. and B.P.G. analyzed the data. S.K.B.T wrote the first draft of the manuscript and, subsequently, S.K.B.T. and B.P.G. worked together to revise it. All authors reviewed the final version. B.P.G. supervised the study.

COMPETING INTERESTS

The authors declare no competing interests.

MATERIALS AND METHODS

Strains and culturing

Strains were cultured on standard NGM (nematode growth media) agar plates using established protocols. Plates were seeded with *E. coli* bacterial strain OP50 as a food source (Brenner 1974). Worms were grown and maintained at the room temperature (20°C) unless stated otherwise. Temperature sensitive strains were grown at their stated temperatures prior to shifting them to 20°C for experiments. See **Supplementary Table 2** for a list of strains used in this study. The wild-type Bristol isolate (N2), which served as a control strain, was obtained from the *Caenorhabditis* Genetics Center (University of Minnesota, St. Paul, MN). Age-synchronized cultures were obtained by using a standard bleaching protocol and treating gravid hermaphrodites with a mixture of sodium hypochlorite and sodium hydroxide (3:2::NaOCl:NaOH) (Brenner 1974).

Plasmid construction and transgenic strains

The plasmid pGLC72 (dat-*1p::YFP)* was described earlier (Salam et al. 2013). Two others, pGLC130 (*hsp::manf-1*) and pGLC180 (*manf-1p::MANF-1::mcherry*), were generated as part of this study. For pGLC130, a 507 bp cDNA fragment of *manf-1* was amplified by PCR using primers GL1041 and GL1042. The fragment was subcloned into pPD49.83 (a gift from Andrew Fire, Addgene plasmid # 1448; http://n2t.net/addgene:1448 ; RRID:Addgene_1448) using *BamH1* and *Nco1* restriction sites. pGLC180 was created by PCR amplification of a 3,429 bp genomic fragment containing 2,713 bp of *manf-1* promoter region and *manf-1* gene (705 bp) using primers GL1749 and GL1750. The fragment was cloned into pHT101 vector (a gift from Casonya Johnson, Addgene plasmid # 61021; http://n2t.net/addgene:61021; RRID: Addgene_61021) using *Pst1* and *Age1* restriction sites.

pGLC130 and pGLC180 were used to generate transgenic strains. pGLC130 (50ng/µL) was injected into the germline of adult N2 hermaphrodites along with the co-injection marker pGLC72 (dat-*1p::YFP*) (50ng/µL). Two independent lines were created DY695 (*bhEx291*) and DY696 (*bhEx292*) (See Supplementary Table 2). DY695 was selected for further use. RT-qPCR analysis showed roughly 15x increase in *manf-1* expression following 1hr heat shock at 31°C. pGLC180 (30ng/µL) was injected along with pGLC72 dat-*1p::YFP* (25ng/µL) co-injection marker. Three independent lines were created DY757 (*bhEx302*), DY758 (*bhEx303*) and DY759 (*bhEx304*) (See **Supplementary Table 2**). RT-qPCR analysis showed 3 to 6-fold increase in *manf-1* expression in each line (data not shown). DY759 was used as a reference strain in this study. pGLC180 was also injected at 10ng/µL and 1ng/µL concentrations to generate DY798 and DY800 strains, respectively.

RNA extraction and RT-qPCR

Total RNA was extracted from adults using Trizol (Catalog Number T9424, Sigma-Aldrich,

Canada). In brief, animals were bleached synchronized at desired adult stages. Worms were collected and washed with M9. Trizol was added followed by flash freezing in liquid nitrogen and then thawed in a 37°C water bath. The flash freeze and thaw step was repeated three to four times. Chloroform was added, mixed and then centrifuged to collect the aqueous phase. Isopropanol was used to precipitate RNA followed by two washes in 75% ethanol. Samples were allowed to air dry to remove any remaining ethanol. Extracted samples were treated with TURBO DNA-free™ Kit (Catalog Number: AM1907, ThermoFisher Scientific) according to manufacturer's instructions. The resulting samples were used to obtain cDNA using the SensiFAST cDNA Synthesis Kit (Catalog Number BIO-65053, MeridianBioscience) following kit instructions.

RT-qPCR was performed (in triplicate) using the Bio-Rad cycler CFX 96 and the SensiFAST SYBR Green Kit (Catalog Number BIO-98005, BIOLINE, USA). Gene expression levels were normalized to housekeeping genes *pmp-3*, *iscu-1* (*Y45F10D.4*) and *cdc-42.* The primers are listed in the **Supplementary File S1**.

qPCR involving Extrachromosomal lines were enriched for fluorescent worms by picking 30 fluorescent day 1 adults and letting them lay eggs overnight. The eggs from these adults were allowed to grow to gravid adults and then bleached to obtain F2 worms. For the DY759 strain, 200 of these F2 fluorescent worms were individually picked at day 1 adult stage after bleach synchronization and were subsequently used for RNA extraction.

RNAi

RNAi-mediated gene silencing was performed using published protcols (Taylor et al. 2021). Knockdowns were performed from the egg stage unless stated otherwise. Worms were fed with empty plasmid (L4440)-containing *E. coli* HT115 culture or gene-specific plasmid culture from the Ahringer library.

Lifespan assay

All lifespan assays were carried out at 20°C on NGM agar plates seeded with *E. coli* OP50 bacteria as previously described (Mallick et al. 2022). All lifespan experiments were repeated in triplicates. Each batch contained roughly 30 animals per strain. Worms were scored every day for survivability starting from day 1 adulthood. They were transferred to fresh plates every other day until no progeny were seen. Cases involving escaping, bursting at vulva, and progeny hatching internally were censored. Survival curves were estimated using the Kaplan-Meir method (see the statistical analysis section).

Heat shock treatments

Animals were grown at room temperature until young adulthood, they were then transferred to a 35°C incubator for 2hrs and assayed for their survival 24hrs later.

hsp::manf-1 transgenic worms (DY695) were age synchronized and grown till adulthood. Day-1 adults were heat shocked at 31°C for 1hr. For lifespan assays, animals were treated every other day starting from day 1 until day 7 of adulthood.

Fluorescence microscopy and quantification

Worms were mounted onto glass slides containing 2% agar pad. Animals were anaesthetized using 30 mM stock solution of NaN_3, if necessary. Fluorescence was visualized using a Zeiss Observer Z1 microscope equipped with an Apotome 2 and X-Cite R 120LED fluorescence illuminator (unless stated otherwise). Fluorescence was quantified using the NIH ImageJ software (*http://rsbweb.nih.gov/ij/*).

Dopaminergic neuron analysis

A previously detailed protocol was adapted to manually score DA neurons (Taylor et al. 2021) using *dat-1p::GFP*. In brief, the neuronal degeneration was scored by counting cell bodies and observing morphologies of cell bodies and dendrites. At least 3 batches of animals were scored with a minimum of 20 animals per batch.

hsp-4p::GFP

Whole animal images were taken to quantify *hsp-4p::GFP* following different conditions. Using the polygon tool of ImageJ, the total fluorescence was obtained. Samples were analyzed in triplicate, a minimum of n = 15 per batch.

α-Synuclein

To quantify α-Synuclein fluorescent intensity, the protocol was adapted from (Richman et al. 2018) and an optimal exposure rate was selected. Images of the head region were taken with the pharynx in focus. Total fluorescent intensity of the head region was obtained using the polygon and measure tool of ImageJ. Samples were analyzed in triplicate, a minimum of n = 15 per batch.

HLH-30::GFP

Intestinal nuclei in day-1 adults were counted for GFP fluorescence using published protocols (Lapierre et al. 2013). As a positive control, animals were allowed to start by transferring them to an unseeded NGM agar plate (no food plate) for 24hrs that induced nuclear location of *hlh-30*. Samples were analyzed in triplicate, a minimum of n = 20 per batch.

polyQ35

To quantify polyQ35 fluorescent intensity and no. of aggregates an optimal exposure rate was selected. Images were taken of the entire worm with the pharynx in focus. Total fluorescent intensity of the head region was obtained using the polygon and measure tool of ImageJ. To

count aggregates the "Find Maxima" function in ImageJ was used. Samples were analyzed in triplicate, a minimum of n = 10 per batch.

LGG-1::GFP

LGG-1 puncta were quantified using a protocol based on published studied (Palmisano and Meléndez 2016; Henis-Korenblit and Meléndez 2019; Kumsta et al. 2019). Z stack images at 63x magnification were taken at optimal slice intervals determined by the Zeiss Zen2 blue software. The maximum projection using Zen2 was acquired and the GFP positive puncta were counted in 4 seam cells per animal. Samples were analyzed in triplicate, a minimum of n = 10 per batch.

SQST-1::GFP

The autophagic flux was quantified using the SQST-1::GFP strain and a protocol based on published studies (Henis-Korenblit and Meléndez 2019; Ploumi et al. 2021). Z stack images were taken at optimal slice intervals determined by the Zeiss Zen2 blue software. A maximum projection of the Z stacks was obtained and GFP positive puncta were counted in the head region using ImageJ "Find Maxima" function. Samples were analyzed in triplicate, a minimum of n = 10 per batch.

Lysosomes

To quantify lysosome numbers and morphology, age synchronized animals were used at the required stages. Z stack images at 63x magnification, ranging from 10 to 15 stacks per image, were taken at optimal slice intervals determined by the Zeiss Zen2 blue software. The maximum projection was created and used to count the number of mCherry-positive foci and to quantify their morphology. The number of mCherry-positive foci per animal were quantified using Cell Profiler (Stirling et al. 2021). The lysosome morphology was grouped into three categories: tubular, intermediate, and vesicular. Chi-square test was used to analyze data.

LysoTracker™ Green staining

LysoTracker™ Green DND-26 dye (Catalog Number: L7526, ThermoFisher Scientific) was used to stain the lysosomes in age synchronized worms as described 16arlier (Sun et al. 2020). A stock solution of 250uM was made. Worms were washed with M9 and placed in a 1.5mL microcentrifuge tube containing 80uL of dye in M9 buffer (working concentration 60µM). The tube was wrapped in an aluminum foil. Animals were placed in a rotator for 1hr and then transferred to an aluminum foil wrapped NGM plate seeded with OP50 bacteria. The plates were placed in the 20°C incubator for 2hrs. Imaged were acquired at 63x magnification and Z stacks were taken.

Oil Red O staining

Neutral lipids in day 1 synchronized adults were visualized by Oil Red O dye (Thermo Fisher Scientific, USA) staining using a published protocol (Ranawade et al. 2018). Images were

acquired using a Nikon 80i Nomarski microscope fitted with a Micropublisher 3.3 RTV color camera and Q imaging software. ImageJ was used to quantify the images (Ranawade et al. 2018). Samples were analyzed in triplicate, n = 15 to 20 animals per batch.

Lipid droplet Imaging

Lipid droplets were quantified using the DHS-3::GFP (Zhang et al. 2012) strain in age synchronized day 1 adults. Z stack images were captured at 63x magnification. The images ranged from 8 to 12 stacks per image at optimal slice intervals determined by the Zeiss Zen2 blue software. As per the published protocol (Clark et al. 2018), a 400µM^2 region of interest was selected in the tail region of worms. All visible lipid droplets were counted, and their diameter was measured using the line tool in Zeiss Zen2 blue software. Samples were analyzed in triplicate, n = 14 per individual batch.

Bodipy 493/503 staining

Bodipy 493/503 (Catalog Number: D3922, Invitrogen) was used to stain lipid droplets in age synchronized worms as described earlier (Klapper et al. 2011). Worms were washed in M9 buffer prior to a 15 minute incubation in 4% fixative (paraformaldehyde solution). Worms were then flash frozen in liquid nitrogen and thawed in a 37°C water bath three times. Animals were then washed with M9 three times to remove fixative. A stock solution of 1mg/mL BODIPY 493/503in DMSO was diluted to a working concentration of 1µg/mL. Worms were then incubated for 1 hour at room temperature in 1µg/mL, after which they were washed three times with M9 and imaged.

Thrashing Assay

The thrashing rate of polyQ35::YFP animals was quantified using a published protocol (Grushko et al. 2021) . Age synchronized day 4 adults were placed in 10uL of M9 buffer and the no. of thrashes in 30 seconds were counted. Samples were analyzed in triplicate, a minimum of n = 15 per batch.

Chemical treatments

Age synchronized day 1 adults were used for chemical treatments unless stated otherwise. Animals were exposed to desired concentrations of drugs on culture plates (Taylor et al. 2021). Acute treatments of tunicamycin and paraquat were carried out in liquid by exposing animals to 50ng/µL and 200mM concentrations, respectively, for 4hrs as described earlier (Mallick et al. 2022). A different tunicamycin concentration of 5µg/mL was used for Fig 1A-C and F-G to measure *manf-1* and *hsp-4* transcripts.

Lifespan assay and ER-UPR reporter *hsp-4p::GFP* assay were performed using existing protocols (Taylor and Dillin 2013). For lifespan, day 1 adults were transferred to plates containing 25ng/µL final concentration of drug. Viability was scored daily. Samples were

analyzed in duplicate, each batch containing a minimum of 30 animals. The *hsp-4p::GFP* animals were placed in a 1.5mL microcentrifuge tube containing 25ng/µL of tunicamycin in M9 buffer and incubated on a rotator for 4hrs. Samples were analyzed in triplicate, each batch containing a minimum of 20 animals.

Statistical analyses

GraphPad Prism 9.5.1 was used to plot all the graphs and perform statistical analysis. A *t*-test or analysis of variance (ANOVA) with a multiple comparison's test was performed depending on the number of conditions and comparisons to be made. Data from repeat experiments were pooled and analyzed together. Graphs are plotted with either SD or SEM and are indicated in figure legends. RT-qPCR results were analyzed using CFX Maestro 3.1 software (Bio-Rad, Canada; https://www.bio-rad.com/en-ca/product/cfx-maestro-software-for-cfx-real-time-pcr-instruments), which performed an ANOVA or *t*-test. SigmaPlot 14 was used to calculate the mean lifespan using the log-rank (Kaplan-Meier) method.

REFERENCES

Abu-Hijleh FA, Prashar S, Joshi H, Sharma R, Frey BN, Mishra RK. 2020. Novel mechanism of action for the mood stabilizer lithium. Bipolar Disord.:1–8. doi:10.1111/bdi.13019.

Altun-Gultekin Z, Andachi Y, Tsalik EL, Pilgrim D, Kohara Y, Hobert O. 2001. A regulatory cascade of three homeobox genes, ceh-10, ttx-3 and ceh-23, controls cell fate specification of a defined interneuron class in C. elegans. Development. 128(11):1951–1969. doi:10.1242/DEV.128.11.1951. [accessed 2023 Jul 19]. https://dx.doi.org/10.1242/dev.128.11.1951.

Bai M, Vozdek R, Hnízda A, Jiang C, Wang B, Kuchar L, Li T, Zhang Y, Wood C, Feng L, et al. 2018. Conserved roles of C. elegans and human MANFs in sulfatide binding and cytoprotection. Nat Commun. 9(1):1–11. doi:10.1038/s41467-018-03355-0.

Bonam SR, Wang F, Muller S. 2019. Lysosomes as a therapeutic target. Nat Rev Drug Discov. 18(12):923–948. doi:10.1038/s41573-019-0036-1. [accessed 2023 May 27]. https://doi.org/10.1038/.

Brenner S. 1974. The Genetics of Caenorhabditis elegans. Genetics. 77:71–94. [accessed 2019 Apr 2]. https://www.ncbi.nlm.nih.gov/pmc/articles/PMC1213120/pdf/71.pdf.

Carosi JM, Fourrier C, Bensalem J, Sargeant TJ. 2022. The mTOR–lysosome axis at the centre of ageing. FEBS Open Bio. 12(4):739–757. doi:10.1002/2211-5463.13347.

Carroll B, Dunlop EA. 2017. The lysosome: A crucial hub for AMPK and mTORC1 signalling. Biochem J. 474(9):1453–1466. doi:10.1042/BCJ20160780. [accessed 2023 Jul 1]. https://pubmed.ncbi.nlm.nih.gov/28408430/.

Clark JF, Meade M, Ranepura G, Hall DH, Savage-Dunn C. 2018. Caenorhabditis elegans DBL-1/BMP regulates lipid accumulation via interaction with insulin signaling. G3 Genes, Genomes, Genet. 8(1):343–351. doi:10.1534/g3.117.300416. [accessed 2023 May 11]. /pmc/articles/PMC5765361/.

Corsi AK, Wightman B, Chalfie M. 2015. A Transparent window into biology : A primer on Caenorhabditis elegans *. WormBook. 200(2):1–31. doi:10.1895/wormbook.1.177.1. [accessed 2020 Oct 21]. /pmc/articles/PMC4492366/?report=abstract.

Danilova T, Belevich I, Li H, Palm E, Jokitalo E, Otonkoski T, Lindahl M. 2019. MANF Is Required for the Postnatal Expansion and Maintenance of Pancreatic b-Cell Mass in Mice. Diabetes. 68:66–80. doi:10.2337/db17-1149. [accessed 2023 Apr 29].

https://doi.org/10.2337/db17-1149.

Danilova T, Galli E, Pakarinen E, Palm E, Lindholm P, Saarma M, Lindahl M. 2019. Mesencephalic Astrocyte-Derived Neurotrophic Factor (MANF) Is Highly Expressed in Mouse Tissues With Metabolic Function. Front Endocrinol (Lausanne). 10:765. doi:10.3389/fendo.2019.00765. [accessed 2020 May 21]. https://www.frontiersin.org/article/10.3389/fendo.2019.00765/full.

Eesmaa A, Yu LY, Göös H, Nõges K, Kovaleva V, Hellman M, Zimmermann R, Jung M, Permi P, Varjosalo M, et al. 2021. The cytoprotective protein MANF promotes neuronal survival independently from its role as a GRP78 cofactor. J Biol Chem. 296:100295. doi:10.1016/j.jbc.2021.100295. [accessed 2021 Mar 1]. https://doi.org/10.1016/j.jbc.2021.100295.

Fares H, Greenwald I. 2001. Genetic analysis of endocytosis in caenorhabditis elegans: Coelomocyte uptake defective mutants. Genetics. 159(1):133–145. doi:10.1093/genetics/159.1.133.

Gee K, Zamora D, Horm T, George L, Upchurch C, Randall J, Weaver C, Sanford C, Miller A, Hernandez S, et al. 2017. Regulators of Lysosome Function and Dynamics in Caenorhabditis elegans. doi:10.1534/g3.116.037515. [accessed 2023 Apr 27]. www.g3journal.org/lookup/suppl/.

Glembotski CC, Thuerauf DJ, Huang C, Vekich JA, Gottlieb RA, Doroudgar S. 2012. Mesencephalic astrocyte-derived neurotrophic factor protects the heart from ischemic damage and is selectively secreted upon sarco/endoplasmic reticulum calcium depletion. J Biol Chem. 287(31):25893–25904. doi:10.1074/jbc.M112.356345.

Grushko D, Boocholez H, Levine A, Cohen E. 2021. Temporal requirements of SKN-1/NRF as a regulator of lifespan and proteostasis in Caenorhabditis elegans. PLoS One. 16(7 July):1–17. doi:10.1371/journal.pone.0243522. http://dx.doi.org/10.1371/journal.pone.0243522.

Hartman JH, Richie CT, Gordon KL, Mello DF, Castillo P, Zhu A, Wang Y, Hoffer BJ, Sherwood DR, Meyer JN, et al. 2019. MANF deletion abrogates early larval Caenorhabditis elegans stress response to tunicamycin and Pseudomonas aeruginosa. Eur J Cell Biol. 98(5–8):1–12. doi:10.1016/j.ejcb.2019.05.002. [accessed 2019 May 31]. https://linkinghub.elsevier.com/retrieve/pii/S0171933518303480.

Henderson MJ, Richie CT, Airavaara M, Wang Y, Harvey BK. 2013. Mesencephalic astrocyte-derived neurotrophic factor (MANF) secretion and cell surface binding are modulated by KDEL receptors. J Biol Chem. 288(6):4209–4225. doi:10.1074/jbc.M112.400648.

Henis-Korenblit S, Meléndez A. 2019. Methods to determine the role of autophagy proteins in C. elegans aging. In: Methods in Molecular Biology. Vol. 1880. Humana Press Inc. p. 561–586. [accessed 2023 Mar 10]. https://link.springer.com/protocol/10.1007/978-1-4939-8873-0_37.

Hetz C, Chevet E, Harding HP. 2013. Targeting the unfolded protein response in disease. Nat Rev Drug Discov. 12(9):703–719. doi:10.1038/nrd3976. [accessed 2020 Oct 20]. www.nature.com/reviews/drugdisc.

Hetz C, Saxena S. 2017. ER stress and the unfolded protein response in neurodegeneration. Nat Rev Neurol. 13(8):477–491. doi:10.1038/nrneurol.2017.99. http://dx.doi.org/10.1038/nrneurol.2017.99.

Jäntti M, Harvey BK. 2020. Trophic activities of endoplasmic reticulum proteins CDNF and MANF. Cell Tissue Res. 382(1):83–100. doi:10.1007/s00441-020-03263-0. [accessed 2021 Mar 11]. https://doi.org/10.1007/s00441-020-03263-0.

Klapper M, Ehmke M, Palgunow D, Böhme M, Matthäus C, Bergner G, Dietzek B, Popp J, Döring F. 2011. Fluorescence-based fixative and vital staining of lipid droplets in Caenorhabditis elegans reveal fat stores using microscopy and flow cytometry approaches. J Lipid Res. 52(6):1281. doi:10.1194/JLR.D011940. [accessed 2022 Oct 6]. /pmc/articles/PMC3090249/.

Kovaleva V, Yu LY, Ivanova L, Shpironok O, Nam J, Eesmaa A, Kumpula EP, Sakson S, Toots U, Ustav M, et al. 2023. MANF regulates neuronal survival and UPR through its ER-located receptor IRE1α. Cell Rep. 42(2). doi:10.1016/j.celrep.2023.112066. [accessed 2023 May 14]. http://www.cell.com/article/S2211124723000773/fulltext.

Kumsta C, Chang JT, Lee R, Tan EP, Yang Y, Loureiro R, Choy EH, Lim SHY, Saez I, Springhorn A, et al. 2019. The autophagy receptor p62/SQST-1 promotes proteostasis and longevity in C. elegans by inducing autophagy. Nat Commun. 10(1):1–12. doi:10.1038/s41467-019-13540-4. [accessed 2022 Sep 13]. https://www.nature.com/articles/s41467-019-13540-4.

Labrousse AM, Zappaterra MD, Rube DA, Van der Bliek AM. 1999. C. elegans dynamin-related protein DRP-1 controls severing of the mitochondrial outer membrane. Mol Cell. 4(5):815–826. doi:10.1016/S1097-2765(00)80391-3. [accessed 2023 Jul 19]. http://www.cell.com/article/S1097276500803913/fulltext.

Lapierre LR, Gelino S, Meléndez A, Hansen M. 2011. Autophagy and lipid metabolism coordinately modulate lifespan in germline-less C. elegans. Curr Biol. 21(18):1507. doi:10.1016/J.CUB.2011.07.042. [accessed 2023 Jul 19]. /pmc/articles/PMC3191188/.

Lapierre LR, De Magalhaes Filho CD, McQuary PR, Chu CC, Visvikis O, Chang JT, Gelino S, Ong B, Davis AE, Irazoqui JE, et al. 2013. The TFEB orthologue HLH-30 regulates autophagy and modulates longevity in Caenorhabditis elegans. Nat Commun. 4. doi:10.1038/NCOMMS3267. [accessed 2022 Aug 30]. /pmc/articles/PMC3866206/.

Lawrence RE, Zoncu R. 2019. The lysosome as a cellular centre for signalling, metabolism and quality control. Nat Cell Biol. 21(2):133–142. doi:10.1038/s41556-018-0244-7. http://dx.doi.org/10.1038/s41556-018-0244-7.

Li Y, Chen B, Zou W, Wang Xin, Wu Y, Zhao D, Sun Y, Liu Y, Chen L, Miao L, et al. 2016. The lysosomal membrane protein SCAV-3 maintains lysosome integrity and adult longevity. J Cell Biol. 215(2):167. doi:10.1083/JCB.201602090. [accessed 2022 Sep 13]. /pmc/articles/PMC5084646/.

Liang JJH, McKinnon IA, Rankin CH. 2020. The contribution of C. elegans neurogenetics to understanding neurodegenerative diseases. J Neurogenet. doi:10.1080/01677063.2020.1803302. [accessed 2020 Aug 18]. https://www.tandfonline.com/doi/abs/10.1080/01677063.2020.1803302.

Lindahl M, Saarma M, Lindholm P. 2017. Unconventional neurotrophic factors CDNF and MANF: Structure, physiological functions and therapeutic potential. Neurobiol Dis. 97:90–102. doi:10.1016/j.nbd.2016.07.009. http://dx.doi.org/10.1016/j.nbd.2016.07.009.

Lindholm P, Peränen J, Andressoo JO, Kalkkinen N, Kokaia Z, Lindvall O, Timmusk T, Saarma M. 2008. MANF is widely expressed in mammalian tissues and differently regulated after ischemic and epileptic insults in rodent brain. Mol Cell Neurosci. 39(3):356–371. doi:10.1016/j.mcn.2008.07.016. http://dx.doi.org/10.1016/j.mcn.2008.07.016.

Lindström R, Lindholm P, Kallijärvi J, Palgi M, Saarma M, Heino TI. 2016. Exploring the conserved role of MANF in the unfolded protein response in Drosophila melanogaster. PLoS One. 11(3):1–18. doi:10.1371/journal.pone.0151550.

Lõhelaid H, Anttila JE, Liew HK, Tseng KY, Teppo J, Stratoulias V, Airavaara M. 2022. UPR Responsive Genes Manf and Xbp1 in Stroke. Front Cell Neurosci. 16:252. doi:10.3389/fncel.2022.900725.

Mallick A, Taylor SKB, Mehta S, Gupta BP. 2022. Cabin1 domain-containing gene picd-1 interacts with pry-1/Axin to regulate multiple processes in Caenorhabditis elegans. Sci Reports 2022 121. 12(1):1–18. doi:10.1038/s41598-022-15873-5. [accessed 2022 Jul 18].

https://www.nature.com/articles/s41598-022-15873-5.

Moncan M, Mnich K, Blomme A, Almanza A, Samali A, Gorman AM. 2021. Regulation of lipid metabolism by the unfolded protein response. J Cell Mol Med. 25(3):1359. doi:10.1111/JCMM.16255. [accessed 2023 Jul 1]. /pmc/articles/PMC7875919/.

Morley JF, Brignull HR, Weyers JJ, Morimoto RI. 2002. The threshold for polyglutamine-expansion protein aggregation and cellular toxicity is dynamic and influenced by aging in Caenorhabditis elegans. Proc Natl Acad Sci U S A. 99(16):10417–10422. doi:10.1073/pnas.152161099. [accessed 2023 Jun 6]. /pmc/articles/PMC124929/.

Napolitano G, Ballabio A. 2016. TFEB at a glance. J Cell Sci. 129(13):2475–2481. doi:10.1242/jcs.146365. [accessed 2023 May 4]. https://journals.biologists.com/jcs/article/129/13/2475/55804/TFEB-at-a-glance.

Nasrolahi A, Mahmoudi J, Akbarzadeh A, Karimipour M, Sadigh-Eteghad S, Salehi R, Farhoudi M. 2018. Neurotrophic factors hold promise for the future of Parkinson's disease treatment: is there a light at the end of the tunnel? Rev Neurosci. 29(5):475–489. doi:10.1515/revneuro-2017-0040.

Neves J, Zhu J, Sousa-Victor P, Konjikusic M, Riley R, Chew S, Qi Y, Jasper H, Lamba DA. 2016. Immune modulation by MANF promotes tissue repair and regenerative success in the retina. Science. 353(6294). doi:10.1126/science.aaf3646.

O'Rourke EJ, Ruvkun G. 2013. MXL-3 and HLH-30 transcriptionally link lipolysis and autophagy to nutrient availability. Nat Cell Biol 2013 156. 15(6):668–676. doi:10.1038/ncb2741. [accessed 2023 Apr 29]. https://www.nature.com/articles/ncb2741.

Pakarinen E and Lindholm P (2023) CDNF and MANF in the brain dopamine system and their potential as treatment for Parkinson's disease. Front. Psychiatry 14:1188697. doi: 10.3389/fpsyt.2023.1188697.

Palgi M, Greco D, Lindström R, Auvinen P, Heino TI. 2012. Gene expression analysis of Drosophilaa Manf mutants reveals perturbations in membrane traffic and major metabolic changes. BMC Genomics. 13(1):134. doi:10.1186/1471-2164-13-134. [accessed 2021 Mar 5]. http://bmcgenomics.biomedcentral.com/articles/10.1186/1471-2164-13-134.

Palmisano NJ, Meléndez A. 2016. Detection of autophagy in Caenorhabditis elegans. Cold Spring Harb Protoc. 2016(2):107–116. doi:10.1101/pdb.top070466.

Peled M, Bar-Lev TH, Talalai E, Aspitz HZ, Daniel-Meshulam I, Bar J, Kamer I, Ofek E, Mor A, Onn A. 2021. Mesencephalic astrocyte-derived neurotrophic factor is secreted from interferon-γ-activated tumor cells through ER calcium depletion. Velasco G, editor. PLoS One. 16(4 April):e0250178. doi:10.1371/journal.pone.0250178. [accessed 2021 Apr 29]. /pmc/articles/PMC8064521/.

Petrova PS, Raibekas A, Pevsner J, Vigo N, Anafi M, Moore MK, Peaire AE, Shridhar V, Smith DI, Kelly J, et al. 2003. MANF A New Mesencephalic, Astrocyte-Derived Neurotrophic Factor with Selectivity for Dopaminergic Neurons. J Mol Neurosci. 20(February):173–187. doi:10.1385/JMN. [accessed 2023 Mar 31]. https://link.springer.com/article/10.1385/JMN:20:2:173.

Ploumi C, Kyriakakis E, Tavernarakis N. 2023. Coupling of autophagy and the mitochondrial intrinsic apoptosis pathway modulates proteostasis and ageing in Caenorhabditis elegans. Cell Death Dis 2023 142. 14(2):1–15. doi:10.1038/s41419-023-05638-x. [accessed 2023 May 4]. https://www.nature.com/articles/s41419-023-05638-x.

Ploumi C, Sotiriou A, Tavernarakis N. 2021. Monitoring autophagic flux in Caenorhabditis elegans using a p62/SQST-1 reporter. In: Methods in Cell Biology. Vol. 165. San Diego [etc.] : Academic Press,. (Monitoring Vesicular Trafficking in Cellular Responses to Stress - Part B). p. 73–87.

Ranawade A, Mallick A, Gupta BP. 2018. PRY-1/Axin signaling regulates lipid metabolism in Caenorhabditis elegans. PLoS One. 13(11):1–22. doi:10.1371/journal.pone.0206540.

Remondelli P, Renna M. 2017. The Endoplasmic Reticulum Unfolded Protein Response in Neurodegenerative Disorders and Its Potential Therapeutic Significance. Front Mol Neurosci. 10:187. doi:10.3389/fnmol.2017.00187. [accessed 2019 Apr 3]. www.frontiersin.org.

Richman C, Rashid S, Prashar S, Mishra R, Selvaganapathy PR, Gupta BP. 2018. C. elegans MANF Homolog Is Necessary for the Protection of Dopaminergic Neurons and ER Unfolded Protein Response. Front Neurosci. 12(AUG):1–11. doi:10.3389/fnins.2018.00544.

Salam S, Ansari A, Amon S, Rezai P, Selvaganapathy PR, Mishra RK, Gupta BP. 2013. A microfluidic phenotype analysis system reveals function of sensory and dopaminergic neuron signaling in C. elegans electrotactic swimming behavior. Worm. 2(2):e24558. doi:10.4161/worm.24558.

Settembre C, De Cegli R, Mansueto G, Saha PK, Vetrini F, Visvikis O, Huynh T, Carissimo A, Palmer D, Jürgen Klisch T, et al. 2013. TFEB controls cellular lipid metabolism through a

starvation-induced autoregulatory loop. Nat Cell Biol 2013 156. 15(6):647–658. doi:10.1038/ncb2718. [accessed 2023 May 4]. https://www.nature.com/articles/ncb2718.

Singh R, Kaushik S, Wang Y, Xiang Y, Novak I, Komatsu M, Tanaka K, Cuervo AM, Czaja MJ. 2009. Autophagy regulates lipid metabolism. Nat 2009 4587242. 458(7242):1131–1135. doi:10.1038/nature07976. [accessed 2023 Jul 1]. https://www.nature.com/articles/nature07976.

Sousa-Victor P, Neves J, Cedron-Craft W, Ventura PB, Liao CY, Riley RR, Soifer I, van Bruggen N, Kolumam GA, Villeda SA, et al. 2019. MANF regulates metabolic and immune homeostasis in ageing and protects against liver damage. Nat Metab 2019 12. 1(2):276–290. doi:10.1038/s42255-018-0023-6. [accessed 2021 Nov 19]. https://www.nature.com/articles/s42255-018-0023-6.

Sousa NS, Brás MF, Antunes IB, Lindholm P, Neves J, Sousa-Victor P. 2023 Mar 23. Aging disrupts MANF-mediated immune modulation during skeletal muscle regeneration. Nat Aging 2023.:1–15. doi:10.1038/s43587-023-00382-5. [accessed 2023 May 4]. https://www.nature.com/articles/s43587-023-00382-5.

Stirling DR, Swain-Bowden MJ, Lucas AM, Carpenter AE, Cimini BA, Goodman A. 2021. CellProfiler 4: improvements in speed, utility and usability. BMC Bioinformatics. 22(1):1–11. doi:10.1186/s12859-021-04344-9. [accessed 2023 Jun 20]. https://bmcbioinformatics.biomedcentral.com/articles/10.1186/s12859-021-04344-9.

Sun Y, Li M, Zhao D, Li X, Yang C, Wang X. 2020. Lysosome activity is modulated by multiple longevity pathways and is important for lifespan extension in C. Elegans. Elife. 9:1–28. doi:10.7554/eLife.55745.

Tadimalla A, Belmont PJ, Thuerauf DJ, Glassy MS, Martindale JJ, Gude N, Sussman MA, Glembotski CC. 2008. Mesencephalic Astrocyte-derived Neurotrophic Factor (MANF) is an Ischemia-inducible Secreted Endoplasmic Reticulum (ER) Stress Response Protein in the Heart. Circ Res. 103(11):1249. doi:10.1161/CIRCRESAHA.108.180679. [accessed 2023 Apr 29]. /pmc/articles/PMC2746824/.

Taylor RC, Dillin A. 2011. Aging as an event of proteostasis collapse. Cold Spring Harb Perspect Biol. 3(5):1–17. doi:10.1101/cshperspect.a004440. [accessed 2021 Nov 9]. http://cshperspectives.cshlp.org/.

Taylor RC, Dillin A. 2013. XBP-1 Is a cell-nonautonomous regulator of stress resistance and longevity. Cell. 153(7):1435. doi:10.1016/j.cell.2013.05.042. [accessed 2020 Mar 25]. http://dx.doi.org/10.1016/j.cell.2013.05.042.

Taylor RC, Hetz C. 2020. Mastering organismal aging through the endoplasmic reticulum proteostasis network. Aging Cell.(June):1–12. doi:10.1111/acel.13265.

Taylor SKB, Minhas MH, Tong J, Selvaganapathy PR, Mishra RK, Gupta BP. 2021. C. elegans electrotaxis behavior is modulated by heat shock response and unfolded protein response signaling pathways. Sci Rep. 11(1):1–17. doi:10.1038/s41598-021-82466-z. https://doi.org/10.1038/s41598-021-82466-z.

The C. elegans Deletion Mutant Consortium. 2012. Large-scale screening for targeted knockouts in the caenorhabditis elegans genome. G3 Genes, Genomes, Genet. 2(11):1415–1425. doi:10.1534/g3.112.003830. [accessed 2020 Dec 6]. www.ncbi.nlm.nih.gov.

Treusch S, Knuth S, Slaugenhaupt SA, Goldin E, Grant BD, Fares H. 2004. Caenorhabditis elegans functional orthologue of human protein h-mucolipin-1 is required for lysosome biogenesis. Proc Natl Acad Sci U S A. 101(13):4483. doi:10.1073/PNAS.0400709101. [accessed 2022 Nov 3]. /pmc/articles/PMC384773/.

Voutilainen MH, Arumäe U, Airavaara M, Saarma M. 2015. Therapeutic potential of the endoplasmic reticulum located and secreted CDNF/MANF family of neurotrophic factors in Parkinson's disease. FEBS Lett. 589(24):3739–3748. doi:10.1016/j.febslet.2015.09.031. http://dx.doi.org/10.1016/j.febslet.2015.09.031.

Voutilainen MH, Back S, Porsti E, Toppinen L, Lindgren L, Lindholm P, Peranen J, Saarma M, Tuominen RK. 2009. Mesencephalic Astrocyte-Derived Neurotrophic Factor Is Neurorestorative in Rat Model of Parkinson's Disease. J Neurosci. 29(30):9651–9659. doi:10.1523/jneurosci.0833-09.2009.

Walter P, Ron D. 2011. The unfolded protein response: From stress pathway to homeostatic regulation. Science. 334(6059):1081–1086. doi:10.1126/science.1209038.

Xu J, Taubert S. 2021. Beyond proteostasis: Lipid metabolism as a new player in er homeostasis. Metabolites. 11(1):1–19. doi:10.3390/metabo11010052. https://doi.org/10.3390/metabo11010052.

Xu N, Zhang SO, Cole RA, McKinney SA, Guo F, Haas JT, Bobba S, Farese R V., Mak HY. 2012. The FATP1-DGAT2 complex facilitates lipid droplet expansion at the ER-lipid droplet interface. J Cell Biol. 198(5):895–911. doi:10.1083/jcb.201201139.

Xu S, Di Z, He Y, Wang R, Ma Y, Sun R, Li J, Wang T, Shen Yujun, Fang S, et al. 2019.

Mesencephalic astrocyte-derived neurotrophic factor (MANF) protects against Aβ toxicity via attenuating Aβ-induced endoplasmic reticulum stress. J Neuroinflammation. 16(35). doi:10.1186/s12974-019-1429-0. [accessed 2019 Nov 16]. https://doi.org/10.1186/s12974-019-1429-0.

Yeawon Kim CL, Chenjian Gu ET, Puri, Anuradhika TAP, Sivapackiam J, Yili Fang, Kendrah Kidd, Sun-Ji Park BGJ, Stanislav Kmoch, Jeremy S. Duffield, Anthony J. Bleyer MEJ, Urano F, Vijay Sharma ML, Chen and YM. 2023. MANF stimulates autophagy and restores mitochondrial homeostasisto treat toxic proteinopathy. Bioarchive.:314–362. https://www.biorxiv.org/content/10.1101/2023.01.10.523171v1.full.pdf.

Zhang P, Na H, Liu Z, Zhang S, Xue P, Chen Y, Pu J, Peng G, Huang X, Yang F, et al. 2012. Proteomic Study and Marker Protein Identification of Caenorhabditis elegans Lipid Droplets. Mol Cell Proteomics. 11(8):317. doi:10.1074/MCP.M111.016345. [accessed 2023 Jul 19]. /pmc/articles/PMC3412964/.

Zhang Y, Grant B, Hirsh D. 2001. RME-8, a Conserved J-Domain Protein, Is Required for Endocytosis in Caenorhabditis elegans. Mol Biol Cell. 12(7):2011. doi:10.1091/MBC.12.7.2011. [accessed 2023 Jul 19]. /pmc/articles/PMC55649/.

Zhang Z, Shen Y, Luo H, Zhang F, Jing L, Wu Y, Xia X, Song Y, Li W, Jin L. 2018. MANF protects dopamine neurons and locomotion defects from a human α-synuclein induced Parkinson's disease model in C. elegans by regulating ER stress and autophagy pathways. Exp Neurol. 308(June):59–71. doi:10.1016/j.expneurol.2018.06.016. https://doi.org/10.1016/j.expneurol.2018.06.016.

Figure legends

Figure 1. Phenotypes observed in *manf-1(tm3603)* following tunicamycin exposure.
(A) Quantification of GFP fluorescence in *manf-1p::gfp* day 1 adults following an 8hr treatment of 5 µg/mL tunicamycin.
(B) *manf*-1 RT-qPCR analysis in day 1 N2 adults following an 8hr treatment of 5 µg/mL tunicamycin.
C) Same as B, except that animals were chronically exposed to 5 µg/mL tunicamycin until day 3 of adulthood.
D) Fluorescent quantification of endogenous MANF-1 in the *MANF-1::mKate2* transgenic strain. Day 1 adults were treated with 25ng/µL tunicamycin overnight.
E) Temporal analysis of GFP fluorescence in *manf-1(tm3603)*; *hsp-4p::GFP* strain with and without 25ng/µL tunicamycin exposure for 4 hours on days 1, 4 and 7 of adulthood.
F) RT-qPCR analysis of *hsp-4* in day-1 *manf-1(tm3603)* adults following an 8hr exposure to 5 µg/mL tunicamycin.
G) Same as F, except that animals were chronically exposed to 5µg/mL tunicamycin until day-3 of adulthood.
H) Representative images *hsp-4p::GFP* fluorescing animals corresponding to the panel E (scale bar 100 µm).
I) Lifespan analysis of *manf-1* mutants and N2 control. N2 mean lifespan 16.0 ± 0.5 days, *manf-1(tm3603)* 14.5 ± 0.4 days and *manf-1(gk3677)* 13.5 ± 0.5 days.
J) Lifespan of animals chronically exposed to 25ng/µL tunicamycin. N2 mean lifespan 10.7 ± 0.3 days, *manf-1(tm3603)* 8.6 ± 0.3 days.
K) Percentage survival following 4hrs exposure to 50ng/µL tunicamycin in liquid.

A, D, E, I-K: 60 – 140 worms (20 worms minimum per batch) from three independent batches. **B, C, F, G**: three independent batches.**A-D, F, G, I**: Results are expressed as mean ± SEM. **E**: Results are expressed as mean ± SD.
Data was analyzed using student's t-test (**A-I**) and the log-rank (Kaplan-Meier) method **(J** and **K)**. *$p<0.05$; **$p<0.01$; ***$p<0.001$; ****$p<0.0001$.

Figure 2. Effect of RNAi knockdown of ER-UPR components on α-Synuclein and polyQ aggregation in *manf-1(tm3603)* animals.
A) RT-qPCR analysis of ER-UPR genes (*atf-6, pek-1,ire-1* and *xbp-1)* in N2 and *manf-1(tm3603)* day 1 adults. *Xbp-1* total and spliced forms are indicated by *xbp-1T* and *xbp-1S*, respectively.
B) The ratio of spliced *xbp-1* to total *xbp-1* in *manf-1(tm3603)* day 1 adults.
C) The fluorescence intensity of α-Synuclein::GFP in body wall muscles of *manf-1(tm3603)* animals was measured in day 1, 4 and 7 adults compared to control.
D-G) α-Synuclein::GFP fluorescent intensities in *manf-1(tm3603)* animals measured on day 1 (D), day 4 (E) and day 7 (F), following RNAi knockdown of *atf-6, pek-1* and *xbp-1***.** L4440 is as an empty vector control RNAi. Representative images for panels D-F are shown in G. Scale bar 100 µm.
H-K) polyQ35 protein aggregation phenotype in *manf-1(tm3603)* animals on day 4 of adulthood compared to wildtype. The total fluorescent intensity measurement of polyQ35::YFP (H) and number of aggregates (I) in body wall muscles. The thrashing response of animals over a 30 second interval (J). Representative Images corresponding to panels H-I. Scale bar 100 µm.

A-B: n = 3 batches of pooled worms. **C-J:** n = 10 to 20 worms per batch (3 batches minimum). **A-B**: Results are mean ± SEM. **C-I:** Results are mean ± SD. **J:** Box plot showing all data points including the mean, and 25th and 75th quartile.
Data was analyzed using student's *t*-test (**A-C, H-J**) and one-way ANOVA with Dunnett's test (**D-F**). *p<0.05; **p<0.01; ***p<0.001; ****p<0.0001. ns: not significant.

Figure 3. *manf-1* overexpression using *hsp::manf-1* confers beneficial effect on animals.
A) RT-qPCR analysis of *manf-1* expression in day 1 *hsp::manf-1* and N2 animals. Animals were either maintained at 20°C or subjected to 1hr heat shock at 31°C.
B) RT-qPCR analysis of day 3 and day 7 *hsp::manf-1* and N2 adults grown at 20°C.
C) Neuronal analysis of *day* 7 *hsp::manf-1* adults. An odd day heat treatment at 31°C starting on day 1 until day 7 was used to activate *hsp::manf-1*. Neurons were categorized as follows, 1: normal (cell bodies and dendrites showing no damage), 2: dendritic damage, 3: cell body missing or abnormally shaped, 4: both dendrites and cell bodies defective.
D) The effect of *hsp::manf-1* overexpression on α-Synuclein aggregation. The fluorescent intensity of α-Synuclein::YFP was measured in day 7 *hsp::manf-1* adults following the same heat treatment as panel C.
E) The lifespan analysis of *hsp::manf-1* animals after being subjected to the same heat treatment as panel C and D. Mean lifespan were 19.0 ± 0.5 days for heat-treated *hsp::manf-1*, 18.1 ± 0.4 days for heat-treated N2 control, 20.2 ± 0.4 days for *hsp::manf-1* with no treatment, and 16.7 ± 0.5 days for N2 control with no treatment.

A-C: three batches. **D,E**: 20-30 worms per batch (3 batches minimum). **A,B,D**: Results are expressed as mean ± SEM.
Data was analyzed using one-way ANOVA with Tukey's test (**A, B**). Chi square test (**C**), Student's *t*-test (**D**), and log-rank (Kaplan-Meier) method (**E**). *$p<0.05$; **$p<0.01$; ***$p<0.001$; ****$p<0.0001$.

Figure 4. Effect of *manf-1* overexpression on neurons, stress response, and the lifespan of animals.

A-B) *hsp-4p::GFP* reporter expression in wildtype, *manf-1(tm3603)*, *MANF-1^{OE}* and *manf-1(tm3603); MANF-1^{OE}* day 1 adults. (A) Quantification of *hsp-4p::*GFP fluorescence; (B) Representative images of *hsp-4::GFP* animals (scale bar 100 µm).

C, D) Analysis of dopaminergic neurons in day 7 *MANF-1^{OE}* adults. (C) Neurons were classified into four different categories based on defects in cell bodies and dendrites. See methods for details. (D) Corresponding images of dopaminergic neurons (scale bar 100 µm).

E, F) The effect of *MANF-1^{OE}* on α-Snuclein::YFP aggregation in body wall muscles of day 4 adults. (E) The α-Synuclein::YFP fluorescence intensity was measured in day 4 *MANF-1^{OE}* adults; (F) Representative images of α-Synuclein::YFP fluorescence in control and MANF-1^{OE} animals at day 4 of adulthood (scale bar 100 µm).

G-J) The effect of *MANF-1^{OE}* on polyQ35::YFP aggregation in body wall muscles of day 4 adults. Quantification of polyQ35::YFP fluorescence intensity (G) and polyQ35::YFP protein aggregates (H). (I) Thrashing response of animals over a 30 second interval. (J) Representative images of day 4 polyQ35::YFP adult animals. Arrows mark aggregates in head of worm. Scale bar 100 µm.

K) Effect of acute tunicamycin exposure (4 hrs at 50 ng/µL) on the survival of wild-type N2 and *MANF-1^{OE}* animals.

L) Lifespan analysis of wild-type N2 and *MANF-1^{OE}* transgenic animals. The mean lifespan for N2 was 16.654 ± 0.368 and *MANF-1^{OE}* animals was 19.907 ± 0.501.

A-I: n = 10 to 30 worms per batch (3 batches minimum). **K:** n = 3 batches of pooled worms. **L:** n = 30 worms per batch, 3 batches. **A, K** is expressed as mean ± SEM. **C-I** is expressed as mean ± SD. **I:** Box plots showing all data points including mean and 25th and 75th quartiles.
Data was analyzed using one-way ANOVA with Tukey's test (**A**), Chi-square test (**C**), Student's *t*-test (**E-K**), and log-rank (Kaplan-Meier) method (**L**). *p<0.05; **p<0.01; ***p<0.001; ****p<0.0001.

Figure 5. MANF-1 expression and colocalization in MANF^{OE} transgenic animals.
A) Fluorescence image of whole worms expressing MANF-1::mCherry reporter at day 1 of adulthood. The hypodermal region is in focus and expression is seen throughout the body. Other prominent areas include the pharynx and coelomocytes. The outlined worm has a dimmer expression of MANF-1::mCherry reporter compared to the worm next to it with a very bright expression. Scale bar 100 µm.
B-D) Enlarged regions showing Z- stacked images of the different areas of MANF-1 expression at day 1 of adulthood. (B) Hypodermal cells. Both fluorescence and bright field merged images are shown. MANF-1::mCherry is seen in clusters of varying sizes, scale bar 20 µm; (C) Diffused fluorescence in the intestinal area and clusters of MANF-1::mCherry in the hypodermal area (scale bar 10 µm); and (D) Coelomocytes showing the bright clusters of MANF-1::mCherry (scale bar 10 µm).
E) MANF-1::mCherry colocalization studies at day 1 of adulthood. The boxed region in the top row has been enlarged and shown below the corresponding image. MANF-1::mCherry colocalized with LysoTracker™ Green DND-26 (hypodermal cells) and lysosomal membrane protein markers LMP-1::GFP (coelomocyte) and SCAV-3::GFP (hypodermal cells). No colocalization was observed with endosome marker RME-8::GFP (coelomocyte) (scale bar 20 µm) and golgi body marker MANS::GFP (coelomocyte). MANS::GFP was imaged using a Leica Confocal (scale bar 10 µm)
F) Quantification of MANF-1::mCherry fluorescing structures in animals shown in G. The foci were analyzed and classified as vesicular, intermediate, or tubular and plotted as a stacked histogram.
G) Fluorescent images of MANF-1^{OE} animals at day 1, 4 and 7 of adulthood. The lower panel shows colocalization using LysoTracker™ Green DND-26. In all images hypodermal cells near the posterior region are shown. Insets show zoomed in view of MANF-1::mCherry foci and their altered morphologies from vesicular to tubular-looking structures in an age dependent manner, scale bar 20 µm.
H) Fluorescent images of endogenous MANF-1 in MANF-1::mKate2 transgenic strain at day 1 of adulthood. The bottom row shows an enlarged view of the white boxed region in the upper panel. The fluorescence is faint and diffused. Regions containing coelomocytes are marked. Treatment with 25ng/µL tunicamycin increased MANF-1 levels, which revealed some overlap with lysosomes (arrowheads), scale bar 20 µm.
F: 10 worms per batch (3 batches minimum) was analyzed using Chi-squared test. *$p<0.05$; **$p<0.01$; ***$p<0.001$; ****$p<0.0001$.

Figure 6. MANF-1^{OE} promotes autophagy clearance and requires HLH-30 to confer neuroprotection and lifespan extension.

A) Quantification of HLH-30::GFP nuclear localization in *MANF-1^{OE}* day 1 adults. Wildtype and starved animals were used as negative and positive controls, respectively. Graph is plotted as cumulative percentage of animals with nuclear localization from 3 batches. The number of animals was as follows: Wildtype 104, *MANF-1^{OE}* 110, and starved 106.

B) RT-qPCR Analysis of *hlh-30, lgg-1* and *sqst-1* transcripts in day 1 wildtype and *MANF-1^{OE}* animals. Only *hlh-30* levels are significant.

C) Quantification of LGG-1::GFP puncta in seam cells of *MANF-1^{OE}* and wildtype day 1 adults.

D) Quantification of SQST-1::GFP puncta in the head region of *MANF-1^{OE}* and wildtype day 1 adults.

E-G) Photomicrographs of animals showing fluorescence of different transgenic reporters at day 1 of adulthood. (E) Representative images corresponding to A showing HLH-30::GFP . Arrows point to areas of intestinal nuclear localization, scale bar 100 µm; (F) Representative images corresponding to C. Fluorescent puncta in LGG-1::GFP seam cells are visible, scale bar 5 µm; and (G) Representative images corresponding to D. SQST-1::GFP puncta in the posterior pharyngeal bulb. Arrows point to puncta in a 30 µm x30 µm region, scale bar 5 µm.

H) Quantification of MANF-1::mCherry foci size in the hypodermis of day 1 *MANF-1^{OE}* and *hlh-30(tm1978); MANF-1^{OE}* adults.

I) Representative images of MANF-1::mCherry foci corresponding to H**,** showing difference in foci size of day 1 adults, scale bar 20 µm.

J) Thrashing rates of *hlh-30(tm1978)* and *hlh-30(tm1978);MANF-1^{OE}* day 4 adults expressing polyQ35::YFP in a 30 second interval.

K) Lifespan analysis of *hlh-30(tm1978)* mutants and *hlh-30(tm1978);MANF-1^{OE}* double at 20°C. Mean lifespan of the different genotypes were as follows: N2 =17.0 ± 0.4 days, *hlh-30(tm1978)* 12.5 ± 0.3 days, *MANF-1^{OE}* 18.5 ± 0.5 days, and *hlh-30(tm1978); MANF-1^{OE}* 13.5 ± 0.2 days.

L) Quantification of lipids in N2 and *manf-1(tm3603)* day 1 adults using Oil Red O staining.

M-P) Quantification of lipids in the intestine of day 1 wildtype and *MANF-1^{OE}* animals using DHS-3::GFP. (M) The normalized GFP fluorescent intensity; (N) The size of lipid droplets in a 400µM^2 area; (O) The number of lipid droplets in a 400µM^2 area; and (P) Representative images of the lipid droplets in the tail region of day 1 adults, scale bar 5 µm.

A: n= 30-40 worms per batch (2-3 batches minimum). **B**: n = 3 batches of pooled worms. **C, D, H and J-O**: 10 to 30 worms per batch (3 batches minimum). **A, B, N, O**: are expressed as mean ± SEM. **C, D, H, L and M** are expressed as mean ± SD. **J:** results are shown as box plots that include mean, minimum, maximum, and 25th and 75th quartile values.

Data was analyzed using one-way ANOVA with Dunnett's test (**A**), Student's t-test (**B-D,H L-O**), one-way ANOVA with Tukey's test (**J**), and log-rank (Kaplan-Meier) method (**K**). *p<0.05; **p<0.01; ***p<0.001; ****p<0.0001.

Figure 1.

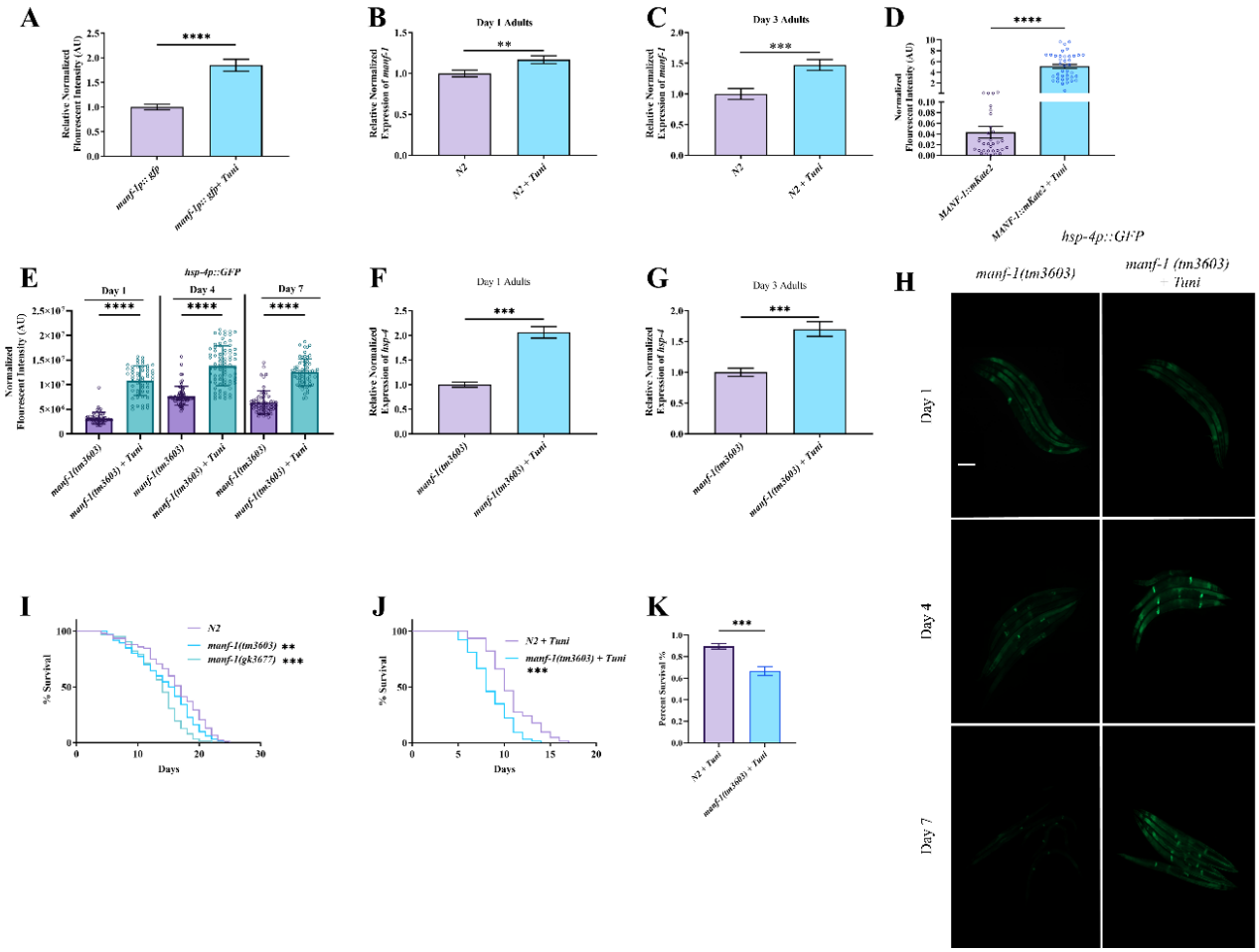
A
Relative Normalized Flourescent Intensity (AU)
****
manf-1p::gfp
manf-1p::gfp+Tuni
B
Day 1 Adults
Relative Normalized Expression of manf-1
**
N2
N2 + Tuni
C
Day 3 Adults
Relative Normalized Expression of manf-1
***
N2
N2 + Tuni
D
Normalized Flourescent Intensity (AU)
****
MANF-1::mKate2
MANF-1::mKate2 + Tuni
E
hsp-4p::GFP
Normalized Flourescent Intensity (AU)
Day 1
Day 4
Day 7
****
****
****
manf-1(tm3603)
manf-1(tm3603) + Tuni
F
Day 1 Adults
Relative Normalized Expression of hsp-4
***
G
Day 3 Adults
Relative Normalized Expression of hsp-4
***
H
hsp-4p::GFP
manf-1(tm3603)
manf-1 (tm3603) + Tuni
Day 1
Day 4
Day 7
I
% Survival
Days
N2
manf-1(tm3603) **
manf-1(gk3677) ***
J
% Survival
Days
N2 + Tuni
manf-1(tm3603) + Tuni ***
K
Percent Survival %
***
N2 + Tuni
manf-1(tm3603) + Tuni

Figure 2.

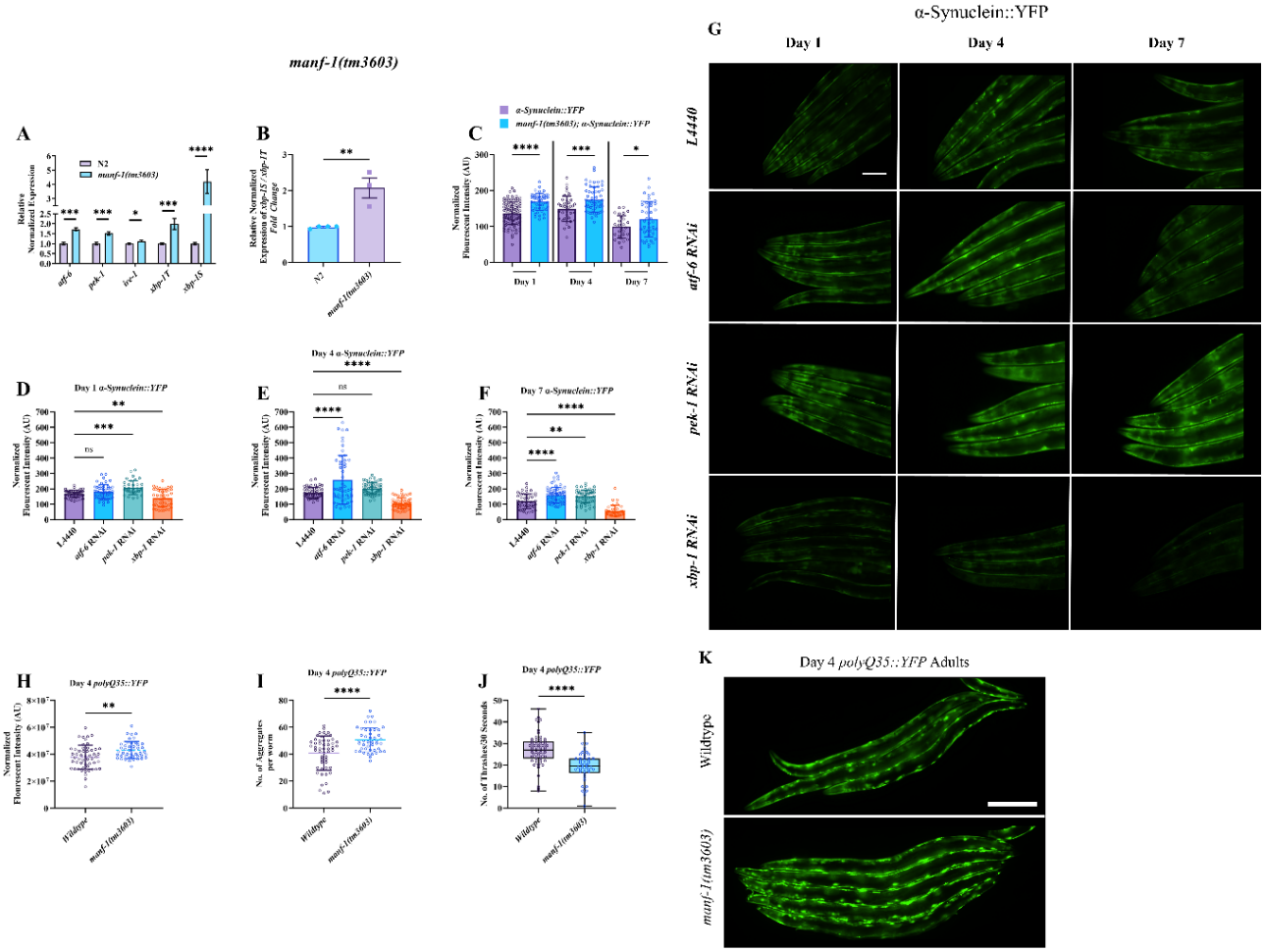
manf-1(tm3603)
A
N2
manf-1(tm3603)
Relative Normalized Expression
atf-6
pek-1
ire-1
xbp-1T
xbp-1S
B
Relative Normalized Expression of xbp-1S / xbp-1T Fold Change
N2
manf-1(tm3603)
C
α-Synuclein::YFP
manf-1(tm3603); α-Synuclein::YFP
Normalized Flourescent Intensity (AU)
Day 1
Day 4
Day 7
D
Day 1 α-Synuclein::YFP
E
Day 4 α-Synuclein::YFP
F
Day 7 α-Synuclein::YFP
L4440
atf-6 RNAi
pek-1 RNAi
xbp-1 RNAi
G
α-Synuclein::YFP
Day 1
Day 4
Day 7
L4440
atf-6 RNAi
pek-1 RNAi
xbp-1 RNAi
H
Day 4 polyQ35::YFP
Normalized Flourescent Intensity (AU)
Wildtype
manf-1(tm3603)
I
Day 4 polyQ35::YFP
No. of Aggregates per worm
J
Day 4 polyQ35::YFP
No. of Thrashes/30 Seconds
K
Day 4 polyQ35::YFP Adults
Wildtype
manf-1(tm3603)

Figure 3.

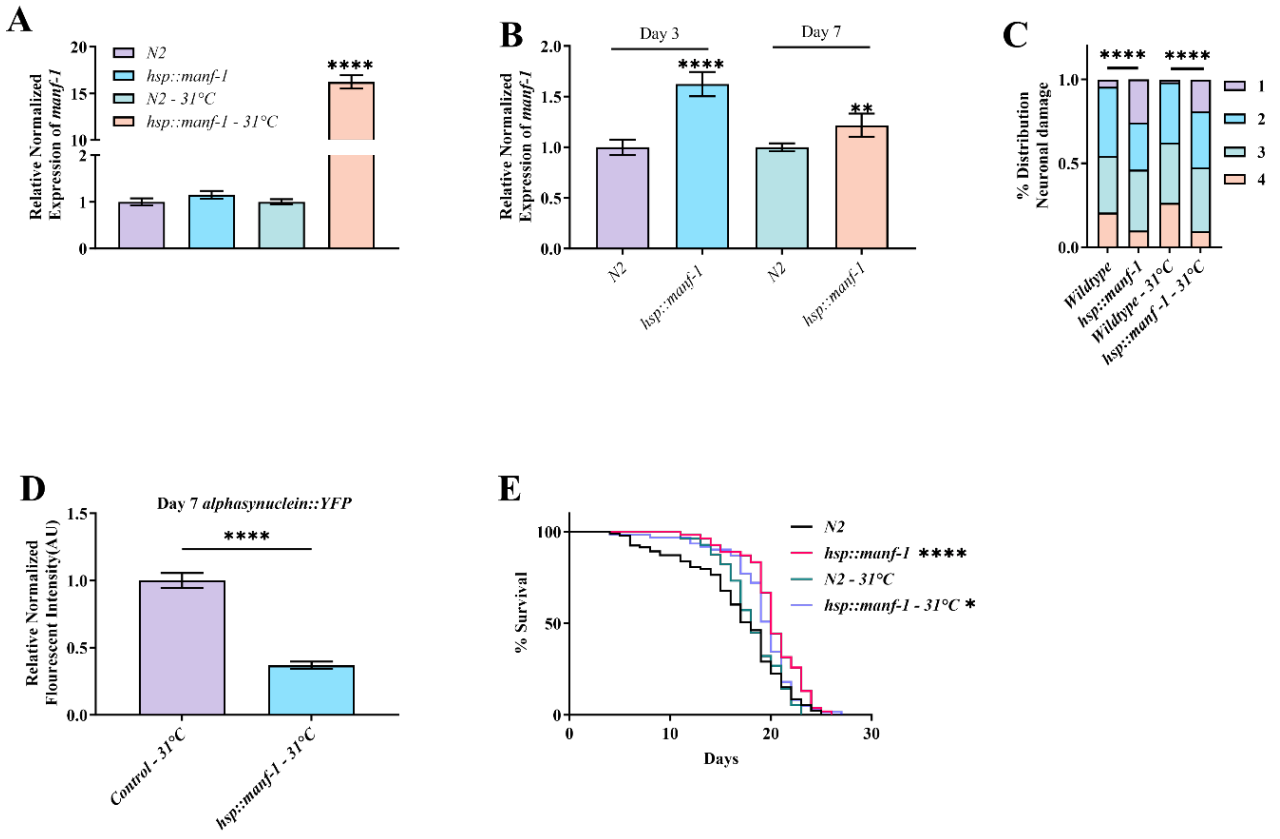
A
Relative Normalized Expression of manf-1
N2
hsp::manf-1
N2 - 31°C
hsp::manf-1 - 31°C
****
B
Day 3
Day 7
Relative Normalized Expression of manf-1
****
**
N2
hsp::manf-1
N2
hsp::manf-1
C
% Distribution Neuronal damage
****
****
1
2
3
4
Wildtype
hsp::manf-1
Wildtype - 31°C
hsp::manf-1 - 31°C
D
Day 7 alphasynuclein::YFP
Relative Normalized Flourescent Intensity(AU)
****
Control - 31°C
hsp::manf-1 - 31°C
E
% Survival
Days
N2
hsp::manf-1 ****
N2 - 31°C
hsp::manf-1 - 31°C *

Figure 4.

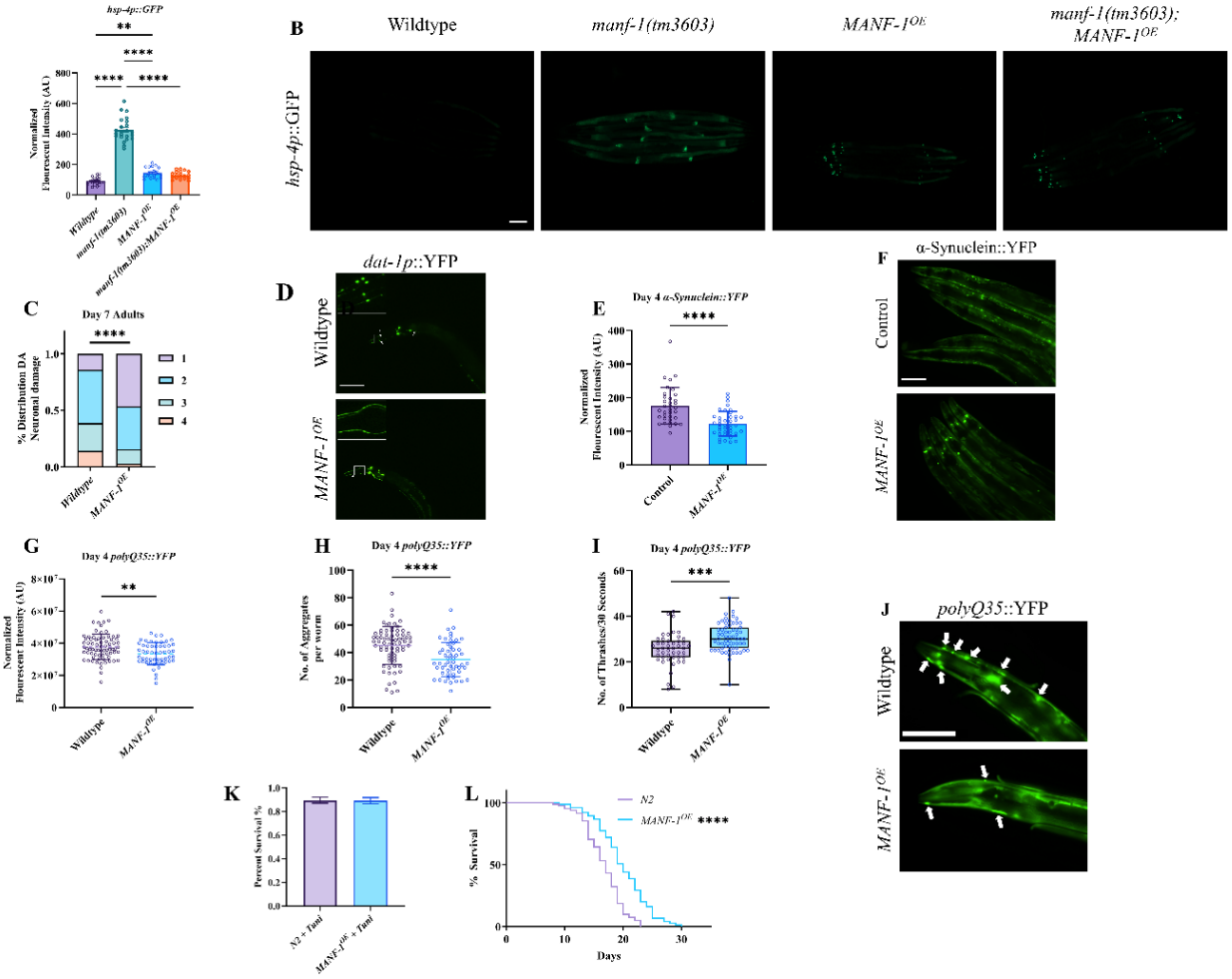
hsp-4p::GFP
Normalized Flourescent Intensity (AU)
Wildtype
manf-1(tm3603)
MANF-1OE
manf-1(tm3603);MANF-1OE
B
Wildtype
manf-1(tm3603)
MANF-1OE
manf-1(tm3603); MANF-1OE
hsp-4p::GFP
C
Day 7 Adults
% Distribution DA Neuronal damage
D
dat-1p::YFP
Wildtype
MANF-1OE
E
Day 4 α-Synuclein::YFP
Normalized Flourescent Intensity (AU)
Control
F
α-Synuclein::YFP
Control
MANF-1OE
G
Day 4 polyQ35::YFP
Normalized Flourescent Intensity (AU)
H
Day 4 polyQ35::YFP
No. of Aggregates per worm
I
Day 4 polyQ35::YFP
No. of Thrashes/30 Seconds
J
polyQ35::YFP
Wildtype
MANF-1OE
K
Percent Survival %
N2 + Tani
MANF-1OE + Tani
L
% Survival
Days
N2
MANF-1OE

Figure 5.

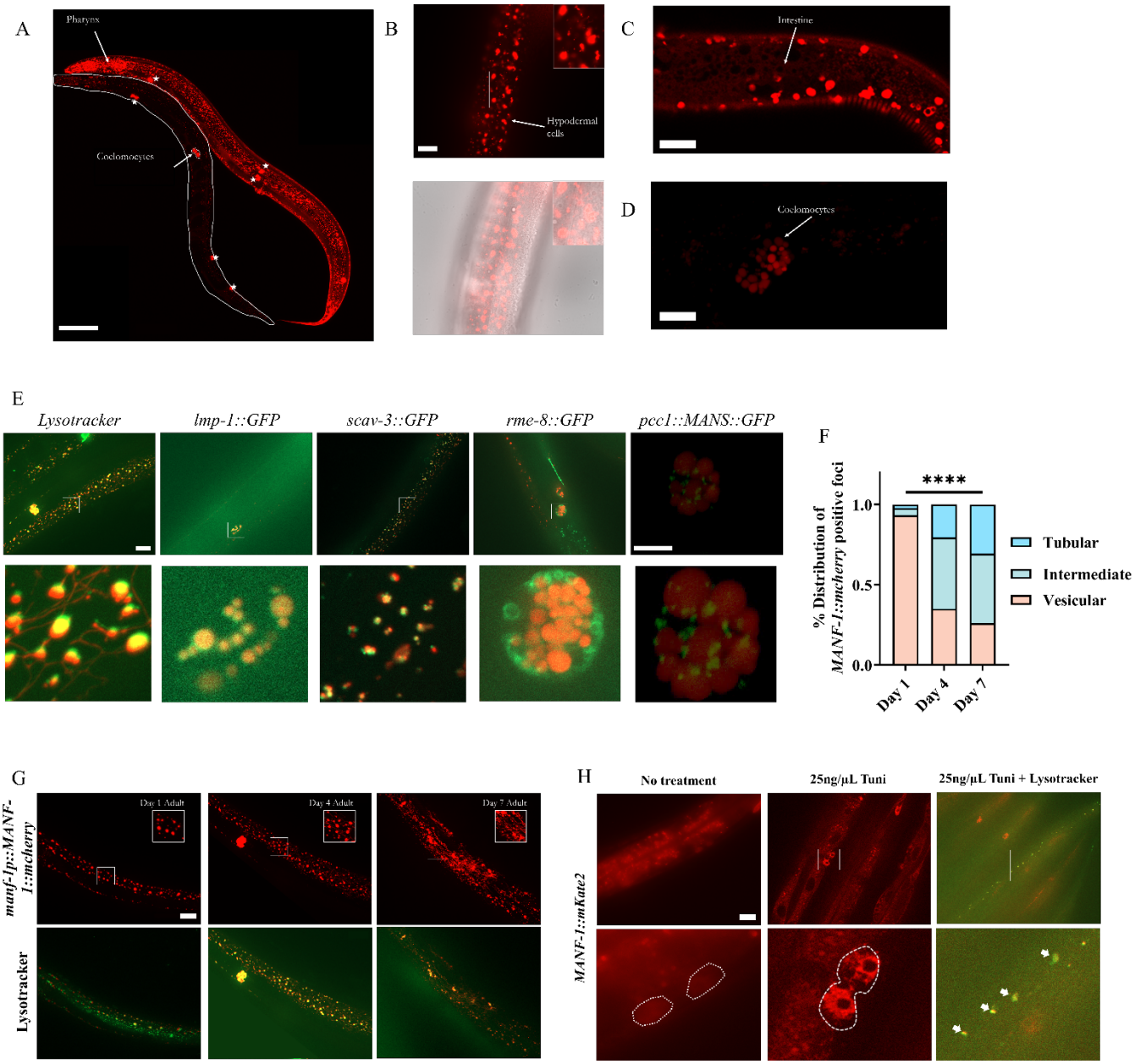
A
Pharynx
Coelomocytes
B
Hypodermal cells
C
Intestine
D
Coelomocytes
E
Lysotracker
lmp-1::GFP
scav-3::GFP
rme-8::GFP
pcc1::MANS::GFP
F
****
% Distribution of MANF-1::mcherry positive foci
1.0
0.5
0.0
Day 1
Day 4
Day 7
Tubular
Intermediate
Vesicular
G
manf-1p::MANF-1::mcherry
Lysotracker
Day 1 Adult
Day 4 Adult
Day 7 Adult
H
No treatment
25ng/µL Tuni
25ng/µL Tuni + Lysotracker
MANF-1::mKate2

Figure 6.

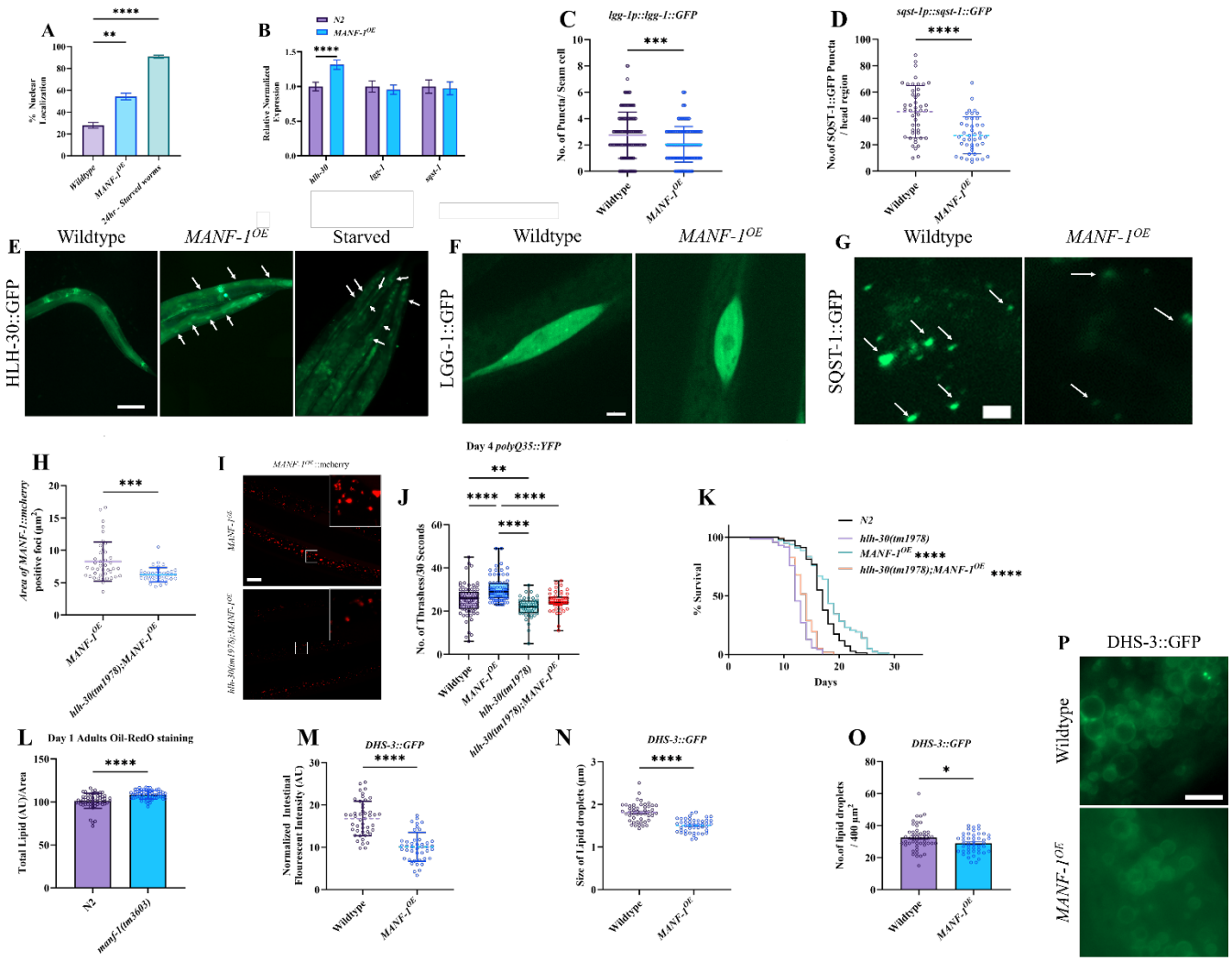
A
% Nuclear Localization
Wildtype
MANF-1OE
24hr - Starved worms
B
N2
MANF-1OE
Relative Normalized Expression
hlh-30
lgg-1
sqst-1
C
lgg-1p::lgg-1::GFP
No. of Puncta/ Seam cell
D
sqst-1p::sqst-1::GFP
No.of SQST-1::GFP Puncta / head region
E
Wildtype
MANF-1OE
Starved
HLH-30::GFP
F
Wildtype
MANF-1OE
LGG-1::GFP
G
Wildtype
MANF-1OE
SQST-1::GFP
H
Area of MANF-1::mcherry positive foci (μm2)
MANF-1OE
hlh-30(tm1978);MANF-1OE
I
MANF-1OE::mcherry
MANF-1OE
hlh-30(tm1978);MANF-1OE
J
Day 4 polyQ35::YFP
No. of Thrashes/30 Seconds
Wildtype
MANF-1OE
hlh-30(tm1978)
hlh-30(tm1978);MANF-1OE
K
N2
hlh-30(tm1978)
MANF-1OE
hlh-30(tm1978);MANF-1OE
% Survival
Days
L
Day 1 Adults Oil-RedO staining
Total Lipid (AU)/Area
N2
manf-1(tm3003)
M
DHS-3::GFP
Normalized Intestinal Flourescent Intensity (AU)
Wildtype
MANF-1OE
N
DHS-3::GFP
Size of Lipid droplets (μm)
Wildtype
MANF-1OE
O
DHS-3::GFP
No.of lipid droplets / 400 μm2
Wildtype
MANF-1OE
P
DHS-3::GFP
Wildtype
MANF-1OE

Supplementary Data

Supplementary Table 1. Lifespan assays. The mean and max lifespan of different genotypes are provided along with treatments. The p values were calculated based on comparison with N2 or respective controls. SEM: Standard Error of Mean. N: number of animals examined.

Genotype	Treatment	Mean Lifespan	SEM	Max Lifespan	N	*p* value
N2	-	16.0	0.5	25	92	-
manf-1(tm3603)	-	14.5	0.4	24	132	0.0183
manf-1(gk3677)	-	13.5	0.5	22	62	0.0000152
N2	25ng/µL tunicamycin	10.7	0.3	17	62	-
manf-1(tm3603)	25ng/µL tunicamycin	8.6	0.3	14	63	<0.001
N2	-	16.7	0.5	25	93	-
hsp::manf-1	-	20.2	0.4	26	54	0.000712
N2	31°C	18.1	0.4	23	56	-
hsp::manf-1	31°C	19.0	0.5	27	61	0.048
N2	-	16.7	0.4	23	81	-
MANF-1^{OE}	-	19.9	0.5	30	75	<0.001
N2	-	17.0	0.4	25	69	-
hlh-30(tm1978)	-	12.5	0.3	17	70	<0.001
MANF-1^{OE}	-	18.5	0.5	29	78	-
MANF-1^{OE}*; hlh-30(tm1978)*	-	13.5	0.2	19	97	<0.001

Supplemental Figure 1. A, B) Age dependent Effect of tunicamycin and paraquat exposure on *manf-1* mutants. Both tunicamycin and paraquat reduced the percentage of viable cell bodies by day 3 and then the damage plateaus. **C)**Heat sensitivity of *manf-1* mutants to 35°C for 2hrs. The survival of worms was checked 24hrs later. *manf-1* mutants exhibited similar survivability compared to N2 worms. **D)** Paraquat resistance of *manf-1* mutants over a 4hr period at a high concentration of 200mM. **A-D:** n = 10 to 30 worms per batch (3 batches minimum), **A-D** is expressed as mean ± SEM. Data was analyzed using two-way ANOVA with Sidak's test (**A and D**) one-way ANOVA with Tukey's test (**B**) and Student's *t*-test (**C**). *p<0.05; **p<0.01; ***p<0.001; ****p<0.0001.

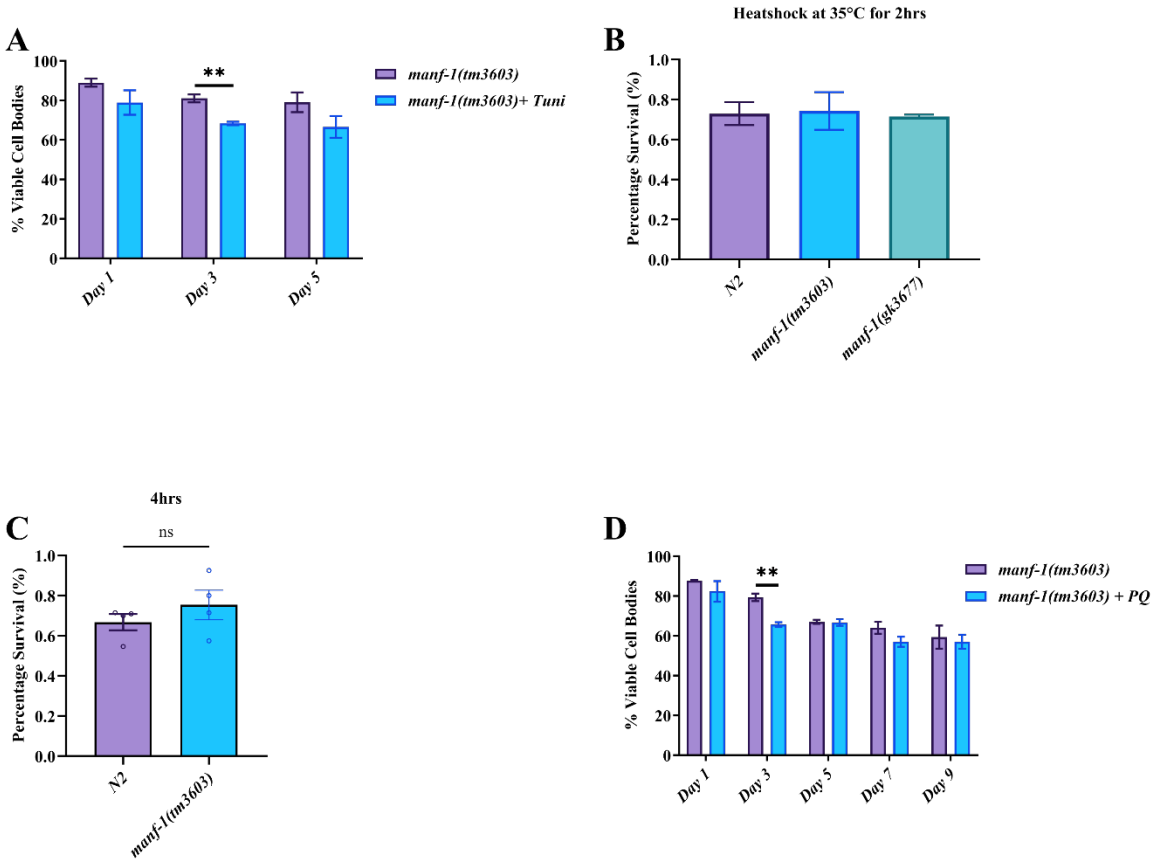

Supplemental Figure 2. *xbp-1* RNAi of *manf-1(tm3603)* animals causes worms to look unhealthy, thin and fragile compared to wildtype animals. The intestine appears to be breaking down on the inside. scale bar 100 µm.

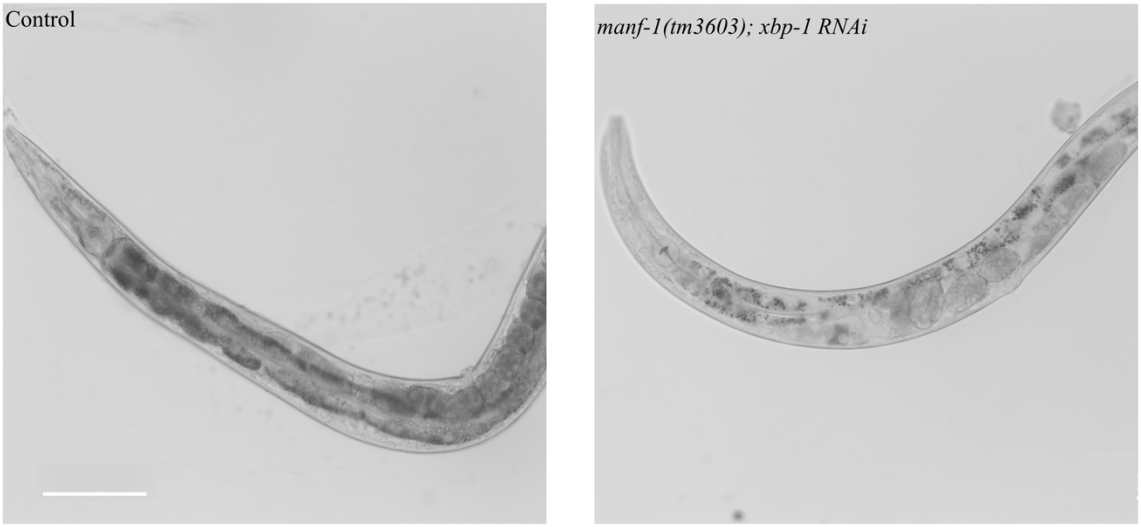

Supplemental Figure 3. The effect of *manf-1(tm3603)* on polyQ40::YFP fluorescent aggregates. The total number of aggregates are significantly increased in *manf-1(tm3063)* animals in day 1 adults compared to wildtype. n = 20 worms (1 batch completed) Data was analyzed using a Student's *t*-test

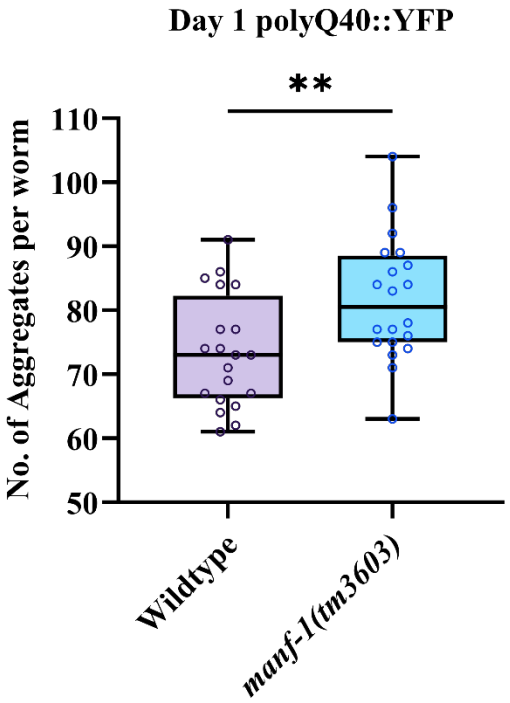

Supplemental Figure 4. Analysis of stress response genes *MANF-1* ^{OE} animals. **A)** qRT-PCR revealed that similar to *manf-1* mutant, *MANF-1* ^{OE} had increased spliced *xbp-1* and total *xbp-1,* but *hsp-4* gene expression was comparable to N2 and *pek-1* was reduced. *Manf-1* transcripts are roughly~6.5 fold increased compared to N2. Results are expressed as mean ± SEM Data was analyzed using student's t-test. (*p<0.05; **p<0.01; ***p<0.001; ****p<0.0001).

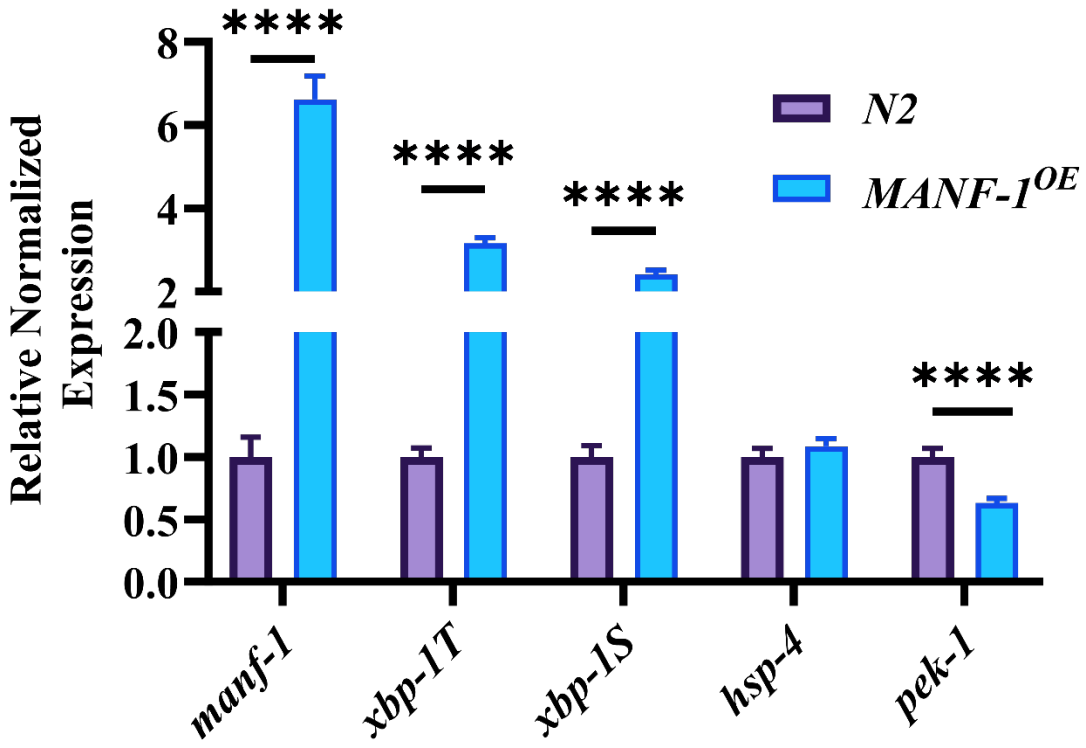
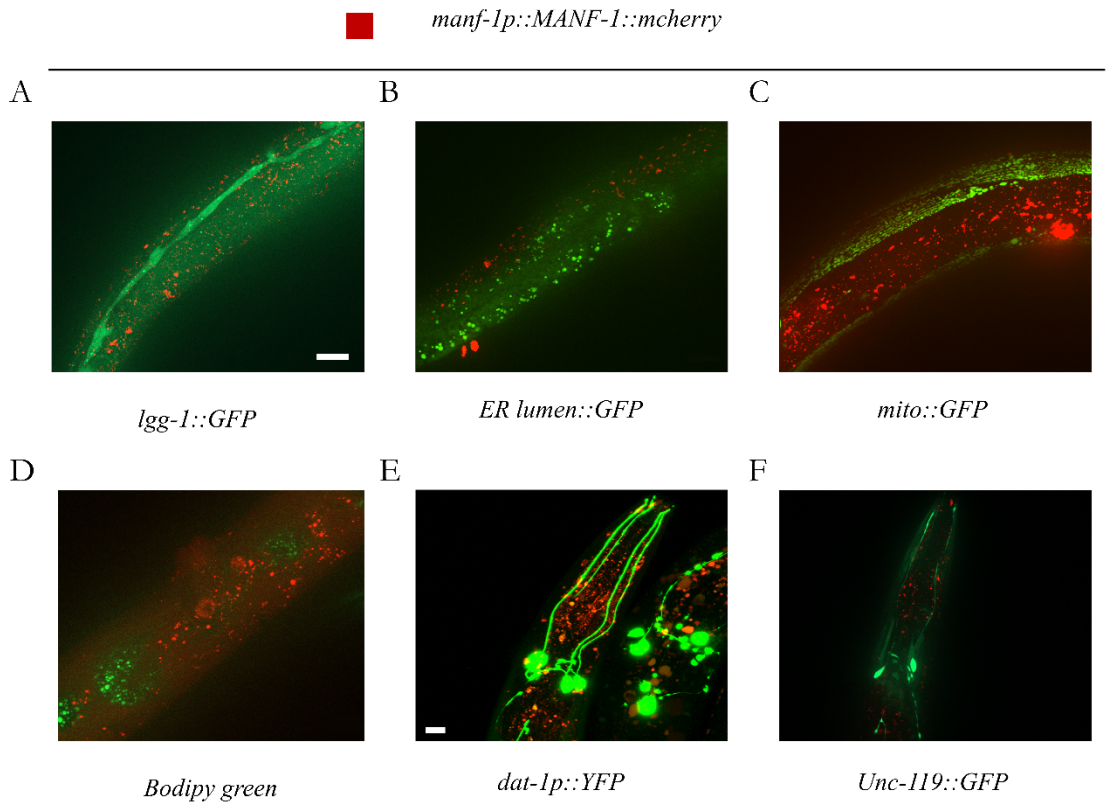
Supplemental Figure 5. Fluorescent analysis of colocalization of MANF-1^{OE} with different subcellular markers. **A-F)** MANF-1^{OE} animals did not show colocalization with the following markers: **A)** autophagosome marker (LGG-1::GFP), **B)** intestinal ER lumen marker (*vha-6p::*GFP::C34B2.10(SP12)), **C)** mitochondria marker (myo-3::GFP(mit)), **D)** lipid droplet marker (*Bodipy 493/503)*, **E)** dopaminergic neurons(*dat-1::YFP)* and **F)** pan neuronal marker (UNC-119::GFP). A-D and F, scale bar 20 µm, E was imaged with a Leica confocal, scale bar 10 µm.